Chemosensory cell-derived acetylcholine drives tracheal mucociliary clearance in response to virulence-associated formyl peptides

Alexander Perniss, Shuya Liu, Brett Boonen, Maryam Keshavarz, Anna-Lena Ruppert, Thomas Timm, Uwe Pfeil, Aichurek Soultanova, Soumya Kusumakshi, Lucas Delventhal, Öznur Aydin, Martina Pyrski, Klaus Deckmann, Torsten Hain, Nadine Schmidt, Christa Ewers, Andreas Günther, Günter Lochnit, Vladimir Chubanov, Thomas Gudermann, Johannes Oberwinkler, Jochen Klein, Katsuhiko Mikoshiba, Trese Leinders-Zufall, Stefan Offermanns, Burkhard Schütz, Ulrich Boehm, Frank Zufall, Bernd Bufe, Wolfgang Kummer

Angaben zur Veröffentlichung / Publication details:

Perniss, Alexander, Shuya Liu, Brett Boonen, Maryam Keshavarz, Anna-Lena Ruppert, Thomas Timm, Uwe Pfeil, et al. 2020. "Chemosensory cell-derived acetylcholine drives tracheal mucociliary clearance in response to virulence-associated formyl peptides." *Immunity* 52 (4): 683–699.e11. https://doi.org/10.1016/j.immuni.2020.03.005.

Chemosensory Cell-Derived Acetylcholine Drives Tracheal Mucociliary Clearance in Response to Virulence-Associated Formyl Peptides

Graphical Abstract

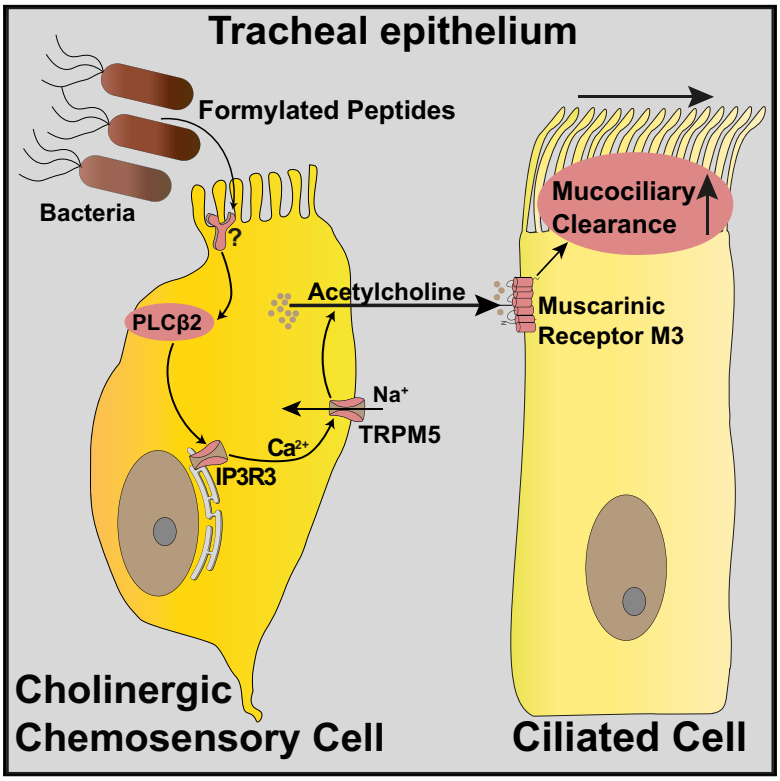

Highlights

- Tracheal chemosensory cells recognize virulence-associated formyl peptides
- This activates a TRPM5-dependent pathway, triggering acetylcholine release
- Acetylcholine released from chemosensory cells activates mucociliary clearance
- Mice with genetic impairment of this pathway are more susceptible to infection

Authors

Alexander Perniss, Shuya Liu, Brett Boonen, ..., Frank Zufall, Bernd Bufe, Wolfgang Kummer

Correspondence

wolfgang.kummer@anatomie.med.uni-giessen.de

In Brief

Cholinergic chemosensory cells are a rare cell type in the tracheal epithelium. Perniss et al. show that they sense formyl peptides from lung pathogenic bacteria and activate a major innate defense mechanism, mucociliary clearance, through acetylcholine release. Deficiency in this pathway is linked to higher susceptibility to infection.

Chemosensory Cell-Derived Acetylcholine Drives Tracheal Mucociliary Clearance in Response to Virulence-Associated Formyl Peptides

Alexander Perniss,[1] Shuya Liu,[2,3] Brett Boonen,[4] Maryam Keshavarz,[1] Anna-Lena Ruppert,[5] Thomas Timm,[6] Uwe Pfeil,[1] Aichurek Soultanova,[1] Soumya Kusumakshi,[7] Lucas Delventhal,[1] Öznur Aydin,[1] Martina Pyrski,[4] Klaus Deckmann,[1] Torsten Hain,[8] Nadine Schmidt,[9] Christa Ewers,[9] Andreas Günther,[10,11] Günter Lochnit,[6] Vladimir Chubanov,[12] Thomas Gudermann,[12] Johannes Oberwinkler,[13] Jochen Klein,[14] Katsuhiko Mikoshiba,[15] Trese Leinders-Zufall,[4] Stefan Offermanns,[2] Burkhard Schütz,[5] Ulrich Boehm,[7] Frank Zufall,[4] Bernd Bufe,[4,16,17] and Wolfgang Kummer[1,17,18,*]

[1]Institute for Anatomy and Cell Biology, German Center for Lung Research, Justus Liebig University, 35385 Giessen, Germany
[2]Department of Pharmacology, Max Planck Institute for Heart and Lung Research, 61231 Bad Nauheim, Germany
[3]Department of Medicine III, University Medical Center Hamburg-Eppendorf, 20251 Hamburg, Germany
[4]Center for Integrative Physiology and Molecular Medicine, Saarland University, 66421 Homburg, Germany
[5]Institute of Anatomy and Cell Biology, Philipps-University, 35037 Marburg, Germany
[6]Institute of Biochemistry, Justus Liebig University, 35385 Giessen, Germany
[7]Experimental Pharmacology, Center for Molecular Signaling (PZMS), Saarland University, 66421 Homburg, Germany
[8]Institute of Medical Microbiology, German Center for Infection Research, Justus Liebig University, 35385 Giessen, Germany
[9]Institute of Hygiene and Infectious Diseases of Animals, Justus Liebig University, 35392 Giessen, Germany
[10]Center for Interstitial and Rare Lung Diseases, Department of Internal Medicine, German Center for Lung Research, Justus Liebig University, 35385 Giessen, Germany
[11]Agaplesion Lung Clinic Waldhof-Elgershausen, 35753 Greifenstein, Germany
[12]Walther-Straub Institute of Pharmacology and Toxicology, German Center for Lung Research, Ludwig-Maximilians-Universität München, 80336 Munich, Germany
[13]Institute of Physiology and Pathophysiology, Philipps-University, 35037 Marburg, Germany
[14]Department of Pharmacology and Clinical Pharmacy, FB14, Goethe University Frankfurt, 60438 Frankfurt am Main, Germany
[15]Laboratory of Cell Calcium Signaling, Shanghai Institute for Advanced Immunochemical Studies, ShanghaiTech University, 201210 Shanghai, China
[16]Department of Informatics and Microsystems Technology, University of Applied Sciences, 67659 Kaiserslautern, Germany
[17]Senior author
[18]Lead Contact
*Correspondence: wolfgang.kummer@anatomie.med.uni-giessen.de
https://doi.org/10.1016/j.immuni.2020.03.005

SUMMARY

Mucociliary clearance through coordinated ciliary beating is a major innate defense removing pathogens from the lower airways, but the pathogen sensing and downstream signaling mechanisms remain unclear. We identified virulence-associated formylated bacterial peptides that potently stimulated ciliary-driven transport in the mouse trachea. This innate response was independent of formyl peptide and taste receptors but depended on key taste transduction genes. Tracheal cholinergic chemosensory cells expressed these genes, and genetic ablation of these cells abrogated peptide-driven stimulation of mucociliary clearance. *Trpm5*-deficient mice were more susceptible to infection with a natural pathogen, and formylated bacterial peptides were detected in patients with chronic obstructive pulmonary disease. Optogenetics and peptide stimulation revealed that ciliary beating was driven by paracrine cholinergic signaling from chemosensory to ciliated cells operating through muscarinic M3 receptors independently of nerves. We provide a cellular and molecular framework that defines how tracheal chemosensory cells integrate chemosensation with innate defense.

INTRODUCTION

Mucociliary clearance is a major innate defense mechanism that removes pathogens from the airways. It is driven by coordinated beating of ciliated cells that comprise a major fraction (25%–65%) of the entire population of epithelial cells (Mercer et al., 1994; Oliveira et al., 2003; Pack et al., 1981). Genetic defects in cilia structure or motility (ciliopathies) are associated with frequent airway infections, highlighting the important physiological role of this defense mechanism (Wijers et al., 2017). Several respiratory pathogens directly attach to cilia (e.g., *Bordetella* species; Opremcak and Rheins, 1983; Perniss et al., 2018; Sekiya et al., 1989) or secrete products that impair ciliary beating (Bailey et al., 2012; Shen et al., 2012), which contributes to their pathogenicity. Conversely, activation of ciliary beating upon contact with microbial products is a desired host response. Despite their potential therapeutic implications, these beneficial

mechanisms are still poorly understood. Current knowledge is largely restricted to human upper airways (nose and sinuses), where ciliated cells directly respond to quorum-sensing molecules (i.e., secreted bacterial pheromones that reflect the population density) generated by *Pseudomonas aeruginosa* and to a yet unidentified product from *Bacillus cereus*, leading to elevated nitric oxide (NO) production. This, in turn, increases ciliary beat frequency in an autocrine manner (Carey et al., 2017; Freund et al., 2018; Lee et al., 2012).

By contrast, the lower airways, from which tracheobronchitis and bronchopneumonia emerge, are far less efficient producers of NO (Dillon et al., 1996), and exhaled NO is reduced rather than elevated in bronchiectasis patients with *P. aeruginosa* infection (Tsang et al., 2002). In addition, ciliated cells of lower airways are much less responsive to NO (Jiao et al., 2011). Yet, particle transport speed (PTS), which is a readout for coordinated ciliary activity in the mouse trachea, was more than doubled by the quorum-sensing molecule from *P. aeruginosa*, N-3-oxododecanoyl-homoserine lactone (3-oxo-C12-HSL) (Krasteva et al., 2012). Hence, NO-independent, currently unidentified mechanisms are likely to play a major role in linking bacterial pathogen recognition to increased ciliary activity in the lower airways.

Here, we identified a subset of bacterial *N*-formyl methionine-containing (fMet) signal peptide fragments corresponding to the N-terminal sequence of proteins from common lung pathogens as activators of mucociliary clearance in the trachea. These peptides activate a rare epithelial cell type, the cholinergic chemosensory cell, expressing the acetylcholine synthesizing enzyme, choline acetyltransferase (ChAT) (Krasteva et al., 2011), and key elements of the taste signaling system, such as the G protein α-gustducin, the phospholipase C isoform β_2 (PLCβ2), and the calcium-activated monovalent cation channel transient receptor potential cation channel subfamily M, member 5 (TRPM5) (Kaske et al., 2007; Krasteva et al., 2011; Tizzano et al., 2011). Cholinergic signaling links such sensory cells to afferent nerve fibers expressing nicotinic acetylcholine receptors (nAChR), resulting in organ-specific reflex responses (Deckmann et al., 2014; Krasteva et al., 2011; Saunders et al., 2014; Tizzano et al., 2010). As acetylcholine is also a major driver of tracheal ciliary activity through the M3 subtype of muscarinic acetylcholine receptors (Klein et al., 2009), we hypothesized that the functional spectrum of chemosensory cell-derived acetylcholine may extend beyond its classical transmitter role, linking chemosensation to mucociliary clearance.

RESULTS

A Bacterial fMet Peptide Motif Drives Ciliary Activity in the Trachea

We screened 18 formylated and 4 unformylated peptides with divergent sequences for ciliotropic activity. These peptides were selected to comprise the synthetic agonist W-peptide (WKYMVm-NH_2) and multiple activators derived from bacterial sequences to stimulate the formyl peptides receptors Fpr1 and Fpr2 that contribute to the initial sensing of infection by immune cells (Bufe et al., 2015). We also used an activator of Fpr3 (f-MKKFRW) recently shown to stimulate infection-avoidance behavior through the olfactory system (Bufe et al., 2019), as well as a broad representation of N termini of bacterial proteins (>1,754 proteins from 18,808 bacterial strains; Table S1). The hexapeptide f-MKKFRW, predominantly contained in the N-terminal sequence of the virulence-associated bacterial protein MgrB (Bufe et al., 2019), but not its unformylated variant MKKFRW, produced a robust increase (76% within 8 min) in PTS on the surface of isolated mouse tracheas with an EC_{50}-value of 0.9 μM (Figures 1A–1C; Video S1). Mean ciliary beat frequency increased from 8.7 to 14.2 Hz within 8 min (Figure 1D).

To determine the sequence selectivity of this effect, we tested several variants of the MgrB N terminus. The extended peptides f-MKKFRWV and f-MKKFRWVVL, as well as the shortened pentapeptide f-MKKFR, all resulted in enhanced PTS (Figures 1A and 1E). Among tested modifications of the core motif (substituted amino acids underlined), f-MKKFRY and f-MKKFKWSI accelerated PTS, whereas no effect was seen with f-MKKWRW, f-MKKHRW, and f-MKRFVWII (Figure 1E). *In silico* analyses (UniProt) revealed the core motif MKKFR and modified PTS-enhancing sequences in a broad spectrum of airway and lung relevant pathogens: *Streptococcus pneumoniae*, *P. aeruginosa*, *Klebsiella pneumoniae*, *K. oxytoca*, *Chlamydia pneumoniae*, *Acinetobacter baumannii*, and *B. bronchiseptica* (Tables S2 and S3).

Cholinergic Chemosensory Cells Drive Peptide-Evoked Mucociliary Clearance through the Canonical Taste Transduction Pathway

Given that TRPM5-expressing solitary chemosensory cells of the upper airways and intestinal tuft cells have been implicated in detection of microbial products (Nadjsombati et al., 2018; Saunders et al., 2014), we reasoned that their tracheal counterpart, the TRPM5-expressing cholinergic chemosensory cell, may mediate the PTS stimulation by fMet peptides. As TRPM5 is a Ca^{2+}-activated monovalent selective cation channel (Hofmann et al., 2003), we developed a tracheal whole-mount preparation in which the genetically encoded Ca^{2+} sensor GCaMP6f is expressed selectively in $TRPM5^+$ cells (Figures 2A and 2B). Exposure to f-MKKFR (50 μM), a peptide that is unable to activate heterologously expressed Fpr3 (Bufe et al., 2019), produced repeatable, transient Ca^{2+} elevations in a subset of the cells (16/102, 16%; n = 5 preparations) (Figure 2C), and 21% (19/92) of cells responded to the MgrB hexapeptide f-MKKFRW (Figure 2D). We also observed cells that responded to both f-MKKFR and f-MKKFRW (n = 4; Figure 2D). For comparison, we stimulated the cells with cycloheximide at two different concentrations, and we applied denatonium at the end of the experiment as a positive control (Figures 2C and 2D). Taken together, these results identified a subset of $TRPM5^+$ tracheal chemosensory cells that recognize PTS-evoking bacterial fMet peptides and respond with intracellular Ca^{2+} elevations.

We next asked whether the $TRPM5^+$ chemosensory cells are required for mediating the stimulatory effect of the fMet peptides on PTS using two different genetic cell ablation models. The transcription factor Pou2f3 is necessary for the development of TRPM5-expressing ($TRPM5^+$) chemosensory cells (Yamashita et al., 2017) and is expressed in mature tracheal cholinergic chemosensory cells (Figure S1A). Tracheas from *Pou2f3*$^{-/-}$ mice lacked $TRPM5^+$ cells (Figure S1B), and the stimulatory effects of both f-MKKFRW and f-MKKFKWSI were nearly absent in such preparations (Figures 2E and 2F).

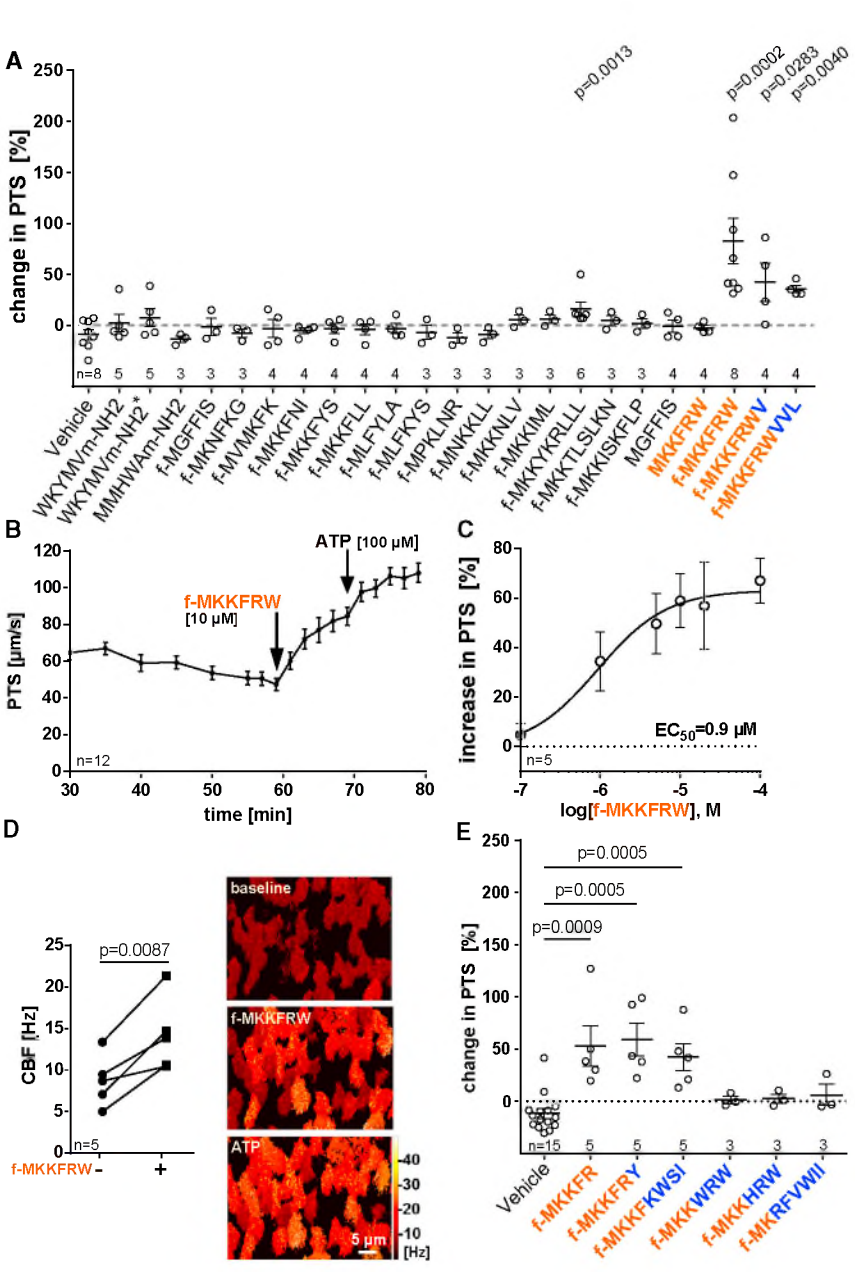

Figure 1. N-Terminal Fragments of Formylated Bacterial Signal Peptides with the Signature f-MKKFR Increase Ciliary Activity

(A) Changes in particle transport speed (PTS) at the murine tracheal surface 8 min after application of different formylated bacterial peptides (10 µM, except 100 µM for WKYMVm-NH2*) and synthetic Fpr agonists (WKYMVm-NH2 and MMHWAm-NH2). The amino acid sequence of the first identified activator, f-MKKFRW, is indicated in all fragments in red letters, with modifications or extensions in blue letters.

(B) PTS at the murine tracheal surface over time. f-MKKFRW (10 µM) was added 59 min after explantation. ATP (100 µM) served as control stimulus to test for viability.

(C) Increase in PTS 8 min after application of f-MKKFRW at ascending concentrations and calculation of EC_{50}.

(D) Ciliary beat frequency (CBF) before (–) and 8 min after (+) application of f-MKKFRW (10 µM), paired t test. Representative images of the tracheal surface and false-color coding of CBF are shown.

(E) Changes in PTS in response to sequence-related derivatives of f-MKKFR (10 µM).

Whiskers show mean ± SEM; PTS data analyzed with Mann-Whitney test against vehicle (HEPES) group.

See also Tables S1, S2, S3, and S4.

loss in cholinergic chemosensory cells in activating cilia-driven transport by f-MKKFRW.

Responses in solitary chemosensory cells to some bacterial metabolites and products can rely on the canonical taste signal transduction cascade downstream of G protein-coupled taste receptors of the Tas1r and Tas2r families (Lee et al., 2014; Saunders et al., 2014; Tizzano et al., 2010). These receptors shared three downstream signaling elements: PLCβ2, which generates inositol-tris-phosphate (IP3), the IP3 receptor isoform 3 (ITPR3), and the calcium-activated monovalent cation channel TRPM5 (Kinnamon, 2012)

Second, we used mice in which the expression of diphtheria toxin A (DTA) is driven by the *Trpm5* promoter. Tracheas of these mice were devoid of epithelial cells displaying immunoreactivity against α-gustducin, PLCβ2, TRPM5, ChAT, and doublecortin-like kinase 1 (DCLK1, a chemosensory cell marker; Bankova et al., 2018) (Figures 2G and S1C–S1F), and f-MKKFRW application failed to stimulate mucosal PTS in these animals (Figure 2H).

Notably, a subset of tracheal epithelial cells characterized by an apical villin-positive tuft (Figures S1C–S1F) and calcitonin gene-related peptide (CGRP)-positive solitary neuroendocrine cells, representing another rare epithelial cell type with chemosensory functions (Gu et al., 2014), persisted in *Trpm5*-DTA mice (Figure 2G). Such cells also remain in *Pou2f3*$^{-/-}$ mice (Yamashita et al., 2017) and therefore represent independent populations, which apparently could not compensate for the (Figure 2I). We found that genetic deletion of each of them fully abrogated the stimulatory effect of f-MKKFRW (Figures 2J–2L). TRPM5 and PLCβ2 are specifically coexpressed in cholinergic chemosensory cells in the mouse trachea (Krasteva et al., 2011). To clarify the cellular distribution of ITPR3, we conducted RT-PCR on cholinergic chemosensory cells and the remaining epithelial cell population isolated by fluorescence-activated cell sorting (FACS) from tracheas of a *Trpm5*-GFP reporter mouse strain (Figure S2). Whereas TRPM5 was specifically expressed in GFP$^+$ cells, ITPR3 was expressed in both GFP$^+$ and GFP$^-$ cells (Figure 2M). To elucidate whether loss of ITPR3 in the ciliated cells themselves caused loss of responsiveness to ciliotropic agents, we directly activated the ciliary cells with muscarine and ATP (Klein et al., 2009). Both molecules still evoked a robust PTS increase in *Itpr3*$^{-/-}$ tracheas (Figures

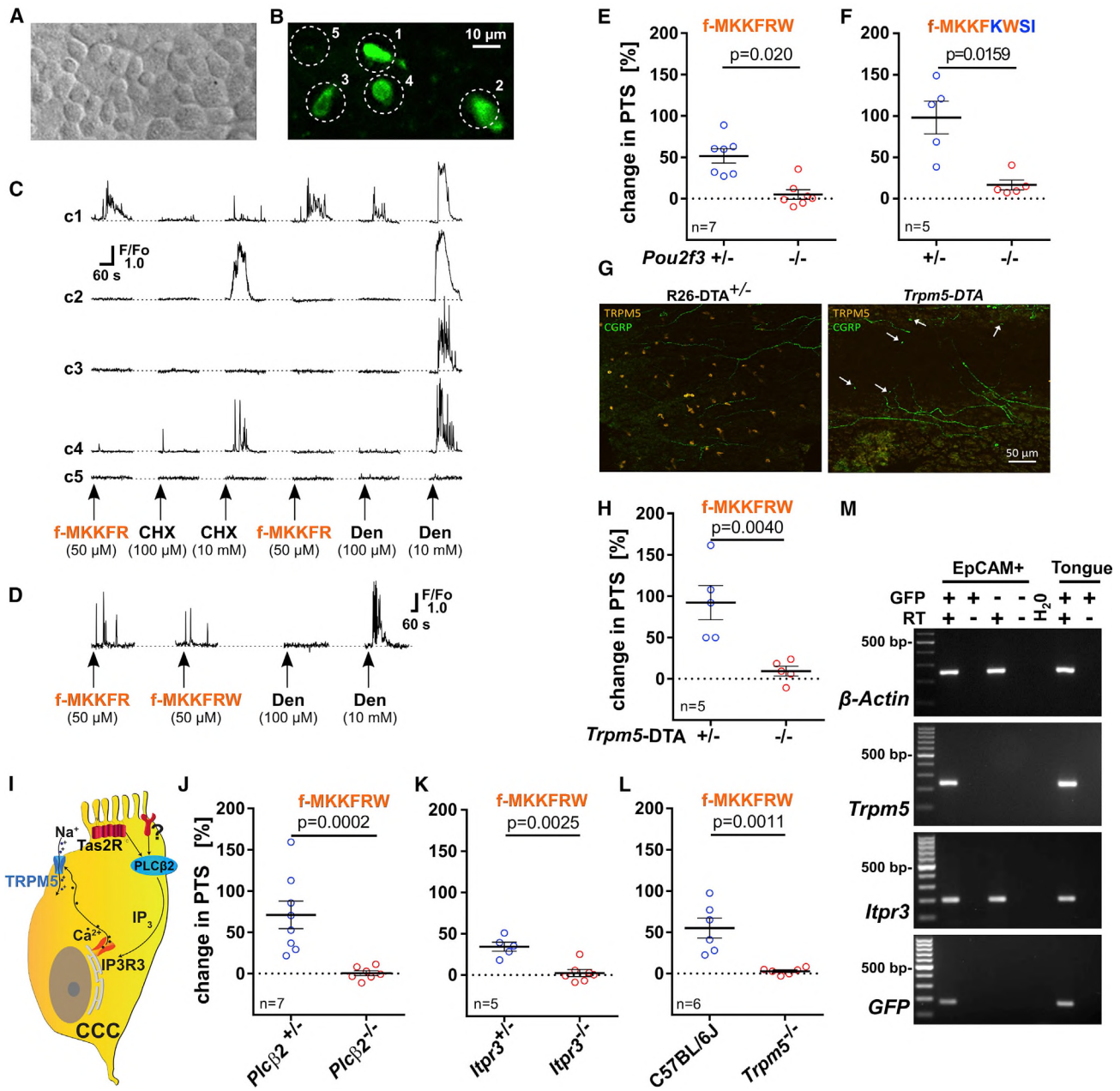

Figure 2. A PLCβ2-IPTR3-Ca^{2+}-TRPM5 Signaling Cascade in Cholinergic Chemosensory Cells Mediates f-MKKFRW-Evoked PTS Stimulation

(A and B) Surface of a tracheal whole-mount preparation used for Ca^{2+} imaging in brightfield overview (A) and in confocal fluorescence mode (B) showing $TRPM5^{+}$ chemosensory cells coexpressing the Ca^{2+} indicator GCaMP6f.

(C) Ca^{2+} responses plotted over time from the individual cells depicted in (B) to successive stimulations with f-MKKFR, cycloheximide (CHX), and denatonium benzoate (Den).

(D) Example of a $TRPM5^{+}$ cell responding to f-MKKFR and f-MKKFRW.

(A–D) Data are representative for experiments in five preparations from four mice.

(E, F, H, and J–L) Increase in PTS in response to f-MKKFRW (10 µM) or f-MKKFKWSI (F) in tracheas from mice lacking TRPM5* chemosensory cells (E, F: *Pou2f3*$^{-/-}$; H: *Trpm5*-DTA) or with deficiency in the chemosensory signal transduction cascade (J: *Plcβ2*$^{-/-}$; K: *Itpr3*$^{-/-}$; L: *Trpm5*$^{-/-}$) and corresponding heterozygous littermate controls (E, F, J, K). *R26-DTA*$^{+/-}$ (R26:lacZbpA^{flox}DTA) mice served as control in (H) and C57BL6/J mice in (L). Whiskers show mean ± SEM, Mann-Whitney test.

(G) Tracheal whole-mount staining with antibodies against TRPM5 and CGRP, labeling single neuroendocrine cells (arrows) and nerve fibers. One trachea per genotype processed as whole mount and further 19 as sections (see also Figure S1C).

(legend continued on next page)

S1G and S1H), indicating that the specific loss of responsiveness to f-MKKFRW resulted from *Itpr3* deletion in the chemosensory cells, not in the ciliated cells.

Activation of Ciliary Activity Occurs Independently of Taste Receptors

The results shown thus far identified a taste-like transduction cascade in cholinergic chemosensory cells as the signaling pathway that is required for f-MKKFRW-driven stimulation of ciliary activity. In lingual taste cells, taste receptors of the Tas1r and Tas2r families function upstream of this pathway (Kinnamon, 2012). Tas1r3, which is expressed in tracheal chemosensory cells (Bankova et al., 2018; Nadjsombati et al., 2018; Tizzano et al., 2011), is an essential component of both umami (Tas1r1-Tas1r3 heterodimers) and sweet receptors (Tas1r2-Tas1r3 heterodimers) (Li et al., 2002; Zhao et al., 2003). Tracheas from *Tas1r3*$^{-/-}$ mice were fully responsive to f-MKKFRW (Figure 3A), and neither sucrose (sweet receptor agonist) nor glutamate (umami receptor agonist) had an impact on ciliary driven transport in wild-type tracheas (Figure 3B). Thus, neither canonical sweet nor umami taste receptors are involved in this effect.

At least 18 of the 35 Tas2r bitter-taste receptors encoded in the mouse genome are expressed in tracheal chemosensory cells (Bankova et al., 2018; Krasteva-Christ et al., 2015; Liu et al., 2017; Montoro et al., 2018; Nadjsombati et al., 2018). Tas2r135 (Bankova et al., 2018; Liu et al., 2017; Nadjsombati et al., 2018) and Tas2r126 (Liu et al., 2017) are particularly highly expressed in this cell type. These two bitter-taste receptors are encoded by the *Tas2r143,Tas2r135,Tas2r126* gene cluster on chromosome 6, and about 85% of tracheal chemosensory cells are labeled in *Tas2r143*-GFP mice (Liu et al., 2017). We generated *Tas2r143*$^{-/-}$*Tas2r135*$^{-/-}$*Tas2r126*$^{-/-}$ compound knockout mice (Figure S3A) and found that the stimulatory effect of f-MKKFRW in tracheas from these mice was partially diminished (44%) (Figure 3C). In view of this partial reduction, we considered the possibility of unspecific effects seen in this triple-receptor-deficient line. Assuming that acetylcholine from chemosensory cells might be involved in the f-MKKFRW driven effect, we tested *Tas2r143*$^{-/-}$*Tas2r135*$^{-/-}$*Tas2r126*$^{-/-}$ mice for intact cholinergic signaling in an independent system. We chose the well-characterized direct cholinergic contraction of the urinary bladder (Stengel et al., 2002). Indeed, muscarine-induced contraction of isolated urinary bladder strips was also significantly diminished (30%) (Figure 3D). These results argued for taste-receptor-unrelated effects affecting muscarinic signaling in this compound knockout line.

We then screened for bitter receptors potentially responding to f-MKKFRW by heterologous expression of 34 mouse Tas2r family members in HEK293T cells. The taste-receptor-expressing cells did not respond with a rise in $[Ca^{2+}]_i$ upon stimulation with f-MKKFRW (Figure 3E). As an independent approach to explore a potential link between bitter receptors expressed by chemosensory cells and PTS activation, we tested a panel of 11 Tas2r agonists on explanted tracheas. These bitter tastants were selected to cover all 10 Tas2r subtypes previously reported to be expressed in tracheal chemosensory cells and for which agonists are known—8 of the 18 Tas2r expressed in chemosensory cells are still orphan receptors—and they covered five additional Tas2r subtypes (Figure 3F). Seven of these agonists were without effect upon PTS or even reduced it (Figures 3F–3H and S3B–S3E). This group included two Tas2r126 agonists (quinine, arbutin), two Tas2r135 agonists (5-propyl-2-thiouracyl, denatonium), and one Tas2r143 agonist (2-propylthiethane) (Lossow et al., 2016; Moine et al., 2018). Together, these results provided further evidence against a substantial role of the receptors of this *Tas2r* cluster in driving ciliary activity. The bitter compound denatonium was tested at five different concentrations. It inhibited PTS at the lowest (0.5 mM) concentration and slightly activated (16%) at the highest concentration (10 mM) (Figure S3E). This high dose, however, drastically reduced the responsiveness to the subsequently applied test stimulus, ATP (Figure S3F). Accelerating effects were obtained with cycloheximide (only by 12%), the *Pseudomonas* quorum-sensing molecule 3-oxo-C12-homoserine lactone, and allylisothiocyanate (Figures S3G–S3K), but all these effects persisted in *pou2f3*$^{-/-}$ tracheas (Figures 3I–3K) and, thus, were not conveyed via TRPM5$^+$ chemosensory cells. The related *Pseudomonas* quorum-sensing molecule 3-oxo-C6-homoserine lactone, which activates nasal TRPM5$^+$ chemosensory cells with an EC_{50} = 80 μM (Tizzano et al., 2010), had no significant effect on PTS at 1–100 μM (Figure S3K).

Activation of Ciliary Activity Occurs Independently of Formyl Peptide Receptors

These data raised the possibility that the responses are mediated by formyl peptide receptors (Fprs). The mouse genome encodes seven known Fprs, of which three (Fpr1, Fpr2 and Fpr3) can be activated by fMet peptides (Bufe et al., 2015; Bufe et al., 2019). We recently identified f-MKKFRW as an Fpr3 agonist (Bufe et al., 2019) and show here that it also activates HEK293T cells expressing Fpr1 and Fpr2 (Figure 4A). Nonetheless, we obtained several lines of evidence that none of these three receptors mediates the f-MKKFRW-triggered increase in ciliary beat frequency. (1) W-peptide, an activator of Fpr1, Fpr2, and Fpr3 at a nanomolar to low micromolar range (Bufe et al., 2012, 2015), did not accelerate PTS, even at 100 μM (Figure 1A). (2) The effect of f-MKKFRW on ciliary-driven transport was insensitive to two established antagonists of Fpr1 and Fpr2, cyclosporin H (1 μM), and tBoc2 (10 μM) (Figure 4B). (3) The effect persisted in FVB/NCrl mice (Figure 4C), which carry an inactivating genomic deletion of bases 424–435 in the *Fpr3* gene (Stempel et al., 2016). (4) The f-MKKFRW effect also persisted in mice with a targeted deletion of either *Fpr1* or *Fpr3* (Figures 4D and 4E). Together, these data ruled out an involvement of Fpr1, Fpr2, and Fpr3 in mediating the ciliotropic effect of f-MKKFRW. The functional properties and agonist profiles of the receptors Fpr-rs3, Fpr-rs4, Fpr-rs6, and Fpr-rs7 are not yet fully established (Liberles et al., 2009; Rivière et al., 2009). We expressed these receptors in HEK293T cells but were unable to observe f-MKKFRW-evoked Ca^{2+} responses

(I) Schematic drawing of the chemosensory signal transduction cascade in cholinergic chemosensory cells (CCC).
(M) RT-PCR of epithelial cells obtained by FACS from *Trpm5*-GFP mice. EpCAM, epithelial cell adhesion molecule; RT ±, samples processed with and without reverse transcriptase; H_2O, sample without cDNA; tongue, positive control. Representative of n = 2.
See also Figures S1 and S2.

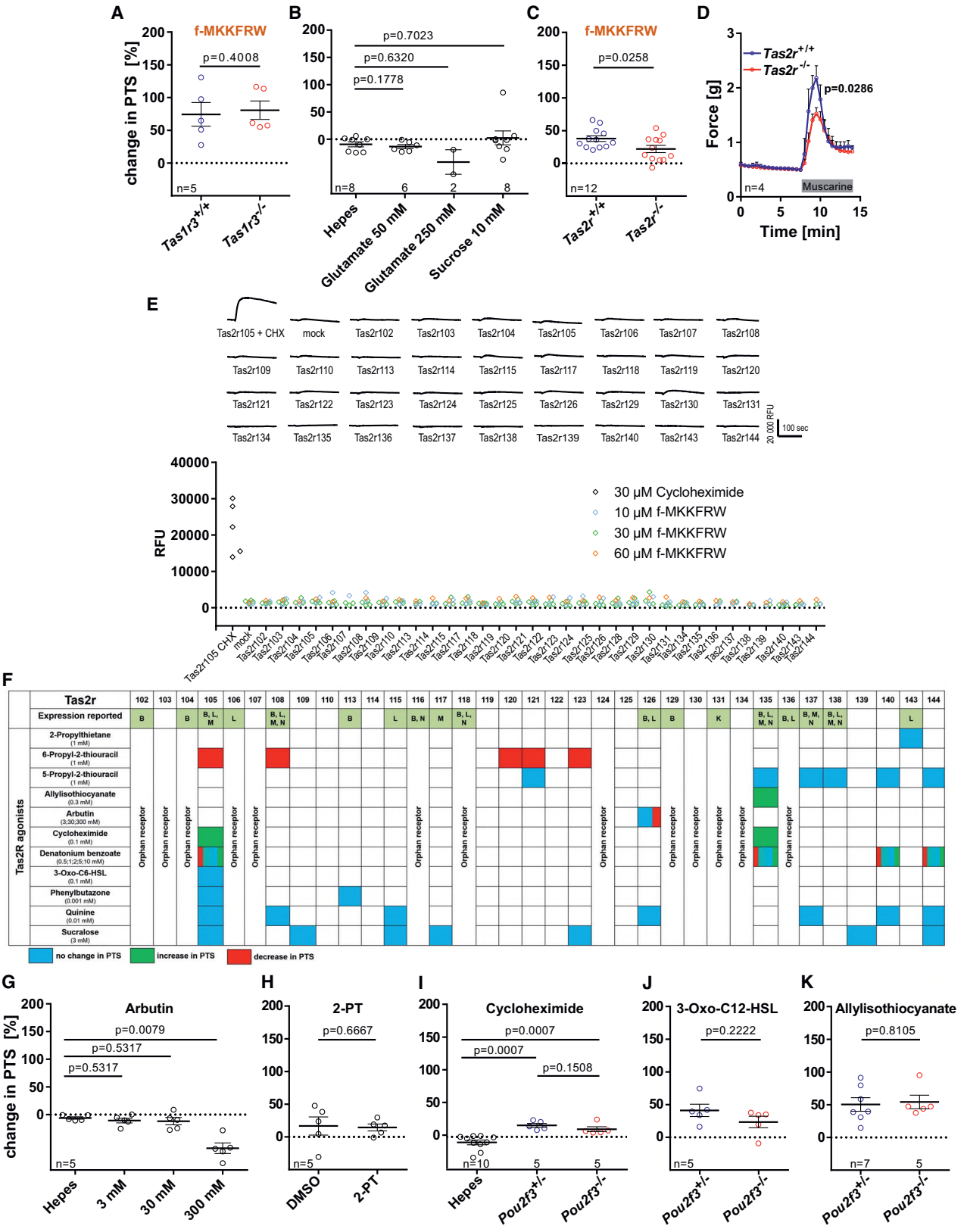

(legend on next page)

(Figure 4A; Table S4). Finally, none of the Fprs were found to be expressed in sorted cholinergic chemosensory cells analyzed by RT-PCR (Figure 4F), and there was no β-gal labeling in tracheas from mice carrying a lacZ-tagged *Fpr3* allele (Bufe et al., 2019) (Figure S4). Collectively, these data indicate that the f-MKKFRW-triggered increase in ciliary beat frequency is independent of Fprs.

Chemosensory Cells Release Acetylcholine upon Stimulation

The loss of f-MKKFRW-stimulated mucosal particle transport in the absence of chemosensory cells implicated a distinct signaling mechanism for communication between chemosensory and ciliated cells rather than direct activation of the ciliated cells. Given that acetylcholine is a powerful activator of PTS in explanted mouse trachea (Klein et al., 2009) and that its synthesizing enzyme ChAT is prominently expressed in tracheal chemosensory cells (Bankova et al., 2018; Krasteva et al., 2011), we examined whether f-MKKFRW triggers acetylcholine release from freshly explanted tracheas (Figure 5A). Indeed, supernatants from tracheas evoked a rise in $[Ca^{2+}]_i$ of CHO cells stably expressing the muscarinic acetylcholine receptor M3, and this effect was sensitive to the muscarinic inhibitor atropine (Figures 5B, 5C, and S5A–S5C). This calcium signal increased 2-fold when tracheas were exposed to f-MKKFRW (Figures 5B and 5C). A significant increase in acetylcholine release upon f-MKKFRW exposure of wild-type tracheas was also measured by high-performance liquid chromatography (HPLC) (Figure 5D), and this effect was absent in both assays when tracheas were taken from *Trpm5*$^{-/-}$ mice (Figures 5C and 5D). These results demonstrate that f-MKKFRW acted through activation of a TRPM5-dependent pathway and strongly suggest the chemosensory cells as the source of acetylcholine.

We next used an optogenetic model of chemosensory cell stimulation to further validate our results, using mice expressing a channelrhodopsin-2 (ChR2)-YFP fusion protein under the control of the *Chat* promoter (Zhao et al., 2011). In tracheas of these mice, we observed native YFP fluorescence in the majority of but not in all cholinergic chemosensory cells, identified by ChAT- and TRPM5-immunolabeling (Figures 5E and S5D–S5F). Immunolabeling with an anti-GFP antibody to visualize lower expression levels of the ChR2-YFP fusion protein increased the number of ChR2-YFP$^+$ cells detected (Figures S5E and S5F). For quantification, we chose colabeling with a TRPM5 antibody, since this proved to be more efficient than ChAT-immunolabeling as tested in a ChAT-GFP reporter mouse strain (Tallini et al., 2006) (Figures S5G and S5H). This approach revealed YFP expression in 82% of TRPM5$^+$ cells (Figure S5F), and no other epithelial cell type displayed YFP (Figures 5E and S5F).

Explanted ChAT-ChR2-YFP and corresponding wild-type tracheas were stimulated with blue light (460 nm), and supernatants taken before and 5 min after stimulation were analyzed for acetylcholine content by HPLC (Figure 5F). LED stimulation of ChAT-ChR2-YFP but not wild-type tracheas evoked a 2-fold increase in acetylcholine in the supernatant (Figures 5G and 5H). This effect required the presence of an intact epithelium, since it was not seen when the epithelium had been mechanically removed prior to the experiment (Figure 5H). Notably, augmented acetylcholine release was accompanied by an increase in PTS (Figure 5I).

As intrinsic parasympathetic neurons also express ChAT (Balentova et al., 2013; Tallini et al., 2006), they also should be considered as a potential source of acetylcholine. In the optogenetic approach, however, there was no evidence for neuronal acetylcholine release, since it was fully dependent on an intact epithelium (Figure 5H). Consistent with this, local ganglion cell somata and nerve endings in the trachealis muscle, the major terminal field of these neurons, did not display native YFP fluorescence, and positive fibers were visible only after YFP immunolabeling (Figure 5J). We used force recordings of tracheal rings in an organ bath preparation to evaluate whether this low expression allowed functional activation of this set of neurons upon illumination with blue light. However, optical stimulation had no effect, even in the presence of eserine, which inhibits the breakdown of acetylcholine through esterases (Figure S5I). This demonstrated that these experimental conditions did not evoke functionally relevant acetylcholine release from nerve terminals, despite proven vitality by electrical field stimulation (EFS) (Figure S5I) and successful optogenetic stimulation in the urinary bladder (Figure S5J). Collectively, these data showed that tracheal chemosensory cells are truly cholinergic and release acetylcholine upon stimulation.

Ciliary Activity Is Driven by Paracrine Cholinergic Signaling from Chemosensory to Ciliated Cells

To clarify the role of this acetylcholine release in conveying the effect of f-MKKFRW on ciliary activity, we generated a mouse line with conditional loss of acetylcholine synthesis in cholinergic chemosensory cells (*Avil*^{cre}*:Chat*$^{fl/fl}$). Tracheas from these mice still retained neural cholinergic signaling, i.e., intact cholinergic constriction evoked by EFS (Figure S6A), and the epithelium still responded to direct application of the cholinergic agonist muscarine (Figure 6A). The effect of f-MKKFRW on PTS, however, was almost fully lost (Figure 6A), providing direct evidence that chemosensory-cell-derived acetylcholine drives ciliary activity.

Figure 3. Activation of Ciliary Activity Occurs Independently of Taste Receptors in Chemosensory Cells

(A–C and G–K) (A–C) Increase in PTS in response to f-MKKFRW (10 μM) or (G–K) taste receptor agonists (concentrations specified in B and F). *Tas2r*$^{-/-}$, triple knockout of *Tas2r143,135,126*; 2-PT = 2-propylthiethane, 3-Oxo-C12-HSL = N-3-oxododecanoyl-homoserine lactone. Whiskers show mean ± SEM, Mann-Whitney test.

(D) Force recording of isolated mouse urinary bladder in response to muscarine (10 μM). Whiskers show mean ± SEM, Mann-Whitney test.

(E) Changes in $[Ca^{2+}]_i$ of HEK293T cells cotransfected with the chimeric G protein alpha subunit G16-Gust44 and a Tas2r receptor or an empty vector (mock). Upper panel: representative time resolved Ca^{2+} transients in response to f-MKKFRW (30 μM). Lower panel: peak Ca^{2+} transients. As positive control, Tas2r105 was stimulated with its agonist cycloheximide (CHX, 30 μM). RFU, relative fluorescence units. Replicates are from six independent experiments.

(F) Summary of previously reported expression of Tas2r family members in tracheal chemosensory cells and effects of Tas2r agonists on PTS as shown in (G)–(K) and Figure S3. Allocation of agonists to receptors is done according to Lossow et al. (2016) and Moine et al. (2018). References for expression are B, Bankova et al. (2018); K, Krasteva-Christ et al. (2015); L, Liu et al. (2017); M, Montoro et al. (2018); N, Nadjsombati et al. 2018).

See also Figure S3.

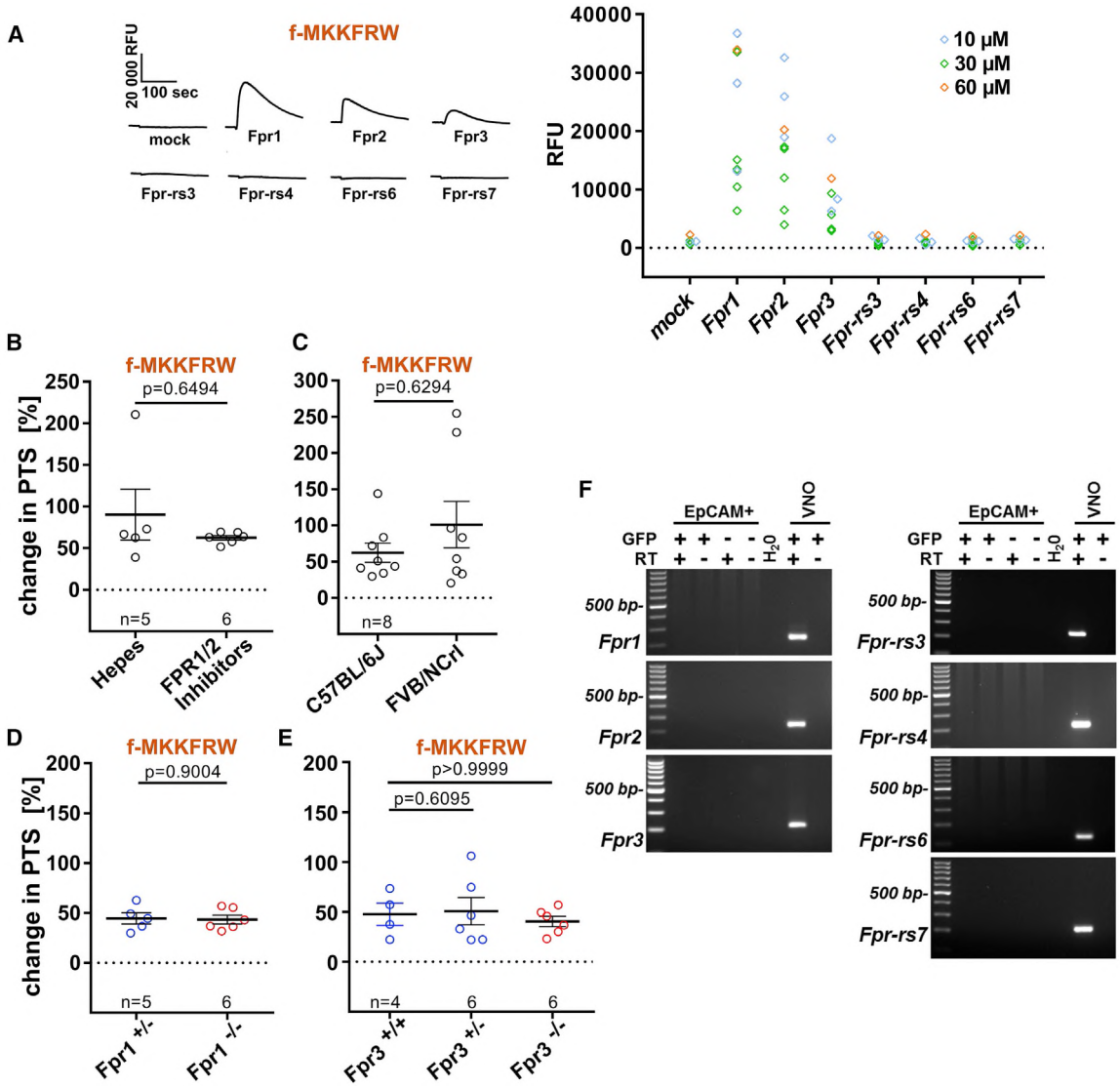

Figure 4. Activation of Ciliary Activity Occurs Independently of Formyl Peptide Receptors

(A) Changes in $[Ca^{2+}]_i$ of HEK293T cell transfected with Fprs or an empty vector (mock) upon stimulation with f-MKKFRW. Left: representative time resolved Ca^{2+} transients of cells in response to f-MKKFRW (10 µM). Right: peak Ca^{2+} transients. Signal amplitudes are given in relative fluorescence units (RFU). Replicates are from six independent experiments.

(B–E) Increase in PTS 8 min after application of f-MKKFRW (10 µM) in C57BL/6J mice without and in presence of a formyl peptide receptor 1 and 2 (Fpr1/2) inhibitor cocktail (cyclosporin H [1 µM] and tBoc2 [10 µM]) (A), in FVB/NCrl mice, which lack a functional Fpr3 (B), and in *Fpr1* (C) and *Fpr3* gene-deficient mice (D). Whiskers show mean ± SEM, Mann-Whitney test.

(F) RT-PCR of cells obtained from FACS-experiments utilizing *Trpm5*-GFP mice. Samples taken from the experiment shown in Figures 2M and S2 and processed in parallel, efficacy control with primers for *β-Actin* shown in Figure 2M. RT ±, samples processed with and without reverse transcriptase; H_2O, sample without cDNA; vomeronasal organ (VNO), positive control. Representative of n = 2.

See also Figures S2 and S4 and Table S4.

This effect may operate either by direct, paracrine action upon muscarinic M3 receptors on ciliated cells (Klein et al., 2009) or indirectly through interposed elements. In particular, some tracheal chemosensory cells are in close apposition to sensory nerve fibers equipped with nAChR containing the subunit α3 (*chrna3*) and the neuropeptide CGRP (Krasteva et al., 2011). In the nose, such fibers were identified as polymodal nociceptors expressing the vanilloid receptor TRPV1 (transient receptor potential cation channel subfamily V, member 1) and releasing the neuropeptide substance P (SP) (Saunders et al., 2014). Stimulation of such peptidergic terminals could also function as a route for increasing ciliary activity (Eljamal et al., 1994). In the explanted trachea preparation, the metabolically stable SP-analog [Sar^9-$Met(O_2)^{11}$]-substance P, but not CGRP, evoked a robust increase in PTS, which was sensitive to inhibition of the SP receptor TACR1 (tachykinin receptor 1, also known as SPR) with RP67580 (Figures 6B and 6C). Thus, nicotinic transmission from cholinergic chemosensory cells to sensory nerve fibers

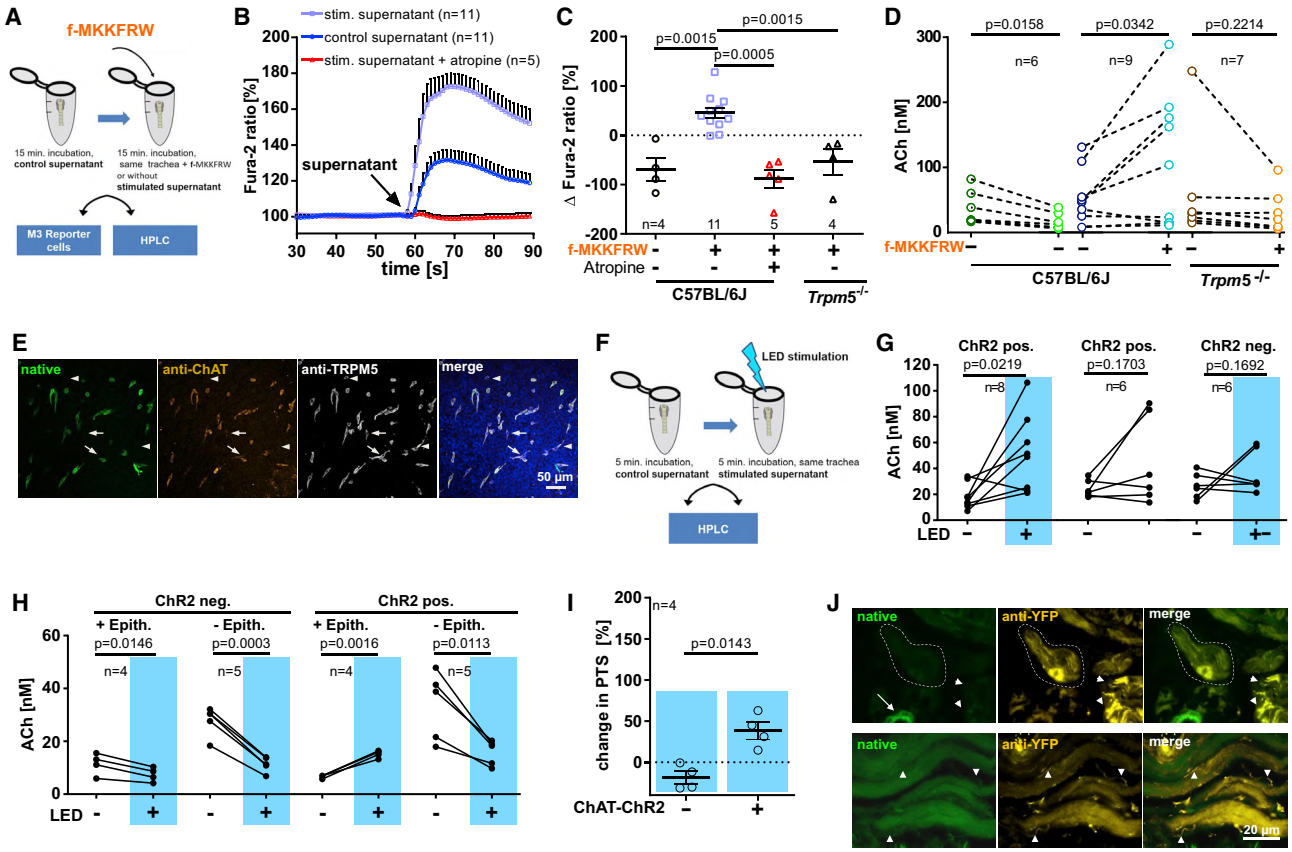

Figure 5. Chemosensory Cells Release Acetylcholine upon Stimulation

(A) Flow chart for obtaining supernatants of tracheas evaluated for acetylcholine content (B–D) after stimulation with f-MKKFRW (10 µM). Control supernatant is taken 15 min after placing the explanted trachea in the reaction tube; stimulated supernatant is taken 15 min after addition of f-MKKFRW or vehicle.

(B) $[Ca^{2+}]_i$ of reporter cells overexpressing the muscarinic M3 receptor in response to tracheal supernatants collected as depicted in (A), recorded as Fura-2 340/380 nm ratio; value immediately before stimulation was set as 100%. Each sample was measured in duplicate in two independent experiments. The general muscarinic inhibitor atropine (1 µM) was added to stimulated supernatants only.

(C) Same experimental setup as shown in (A) and (B). Δ-Values indicate the difference in signal increases evoked by supernatants taken from the first 15 min incubation period (in all cases without stimulants, shown on the left in A) and supernatants taken from the second 15 min incubation period (on the right in A), with and without f-MKKFRW as indicated. Atropine, if indicated, was added to the reporter cells during recording. Negative values represent a reduction in acetylcholine content over the incubation period; positive values reflect acetylcholine release. Whiskers show mean ± SEM, Mann-Whitney test.

(D) Acetylcholine (ACh) concentration in supernatants of unstimulated (f-MKKFRW –) and stimulated (f-MKKFRW +) tracheas from C57BL/6J and *Trpm5*$^{-/-}$ mice measured by HPLC; Wilcoxon matched-pairs signed rank test.

(E) Tracheal whole-mount immunostaining showing endogenous, native ChR2-YFP expression (green) and antibody staining for ChAT (orange) and for TRPM5 (gray) in a ChAT-ChR2-YFP trachea. In the merged image, nuclei are stained blue with DAPI. C57BL/6J trachea processed as control is depicted in Figure S5D. Representative for five tracheas of each genotype stained in two independent experiments.

(F) Flow chart for obtaining supernatants of tracheas evaluated for acetylcholine content in optogenetic experiments; "control" and "stimulated" defined as in (A).

(G) Acetylcholine content, measured by HPLC, in tracheal supernatants before and after LED stimulation or in two supernatants taken at the same time intervals without LED stimulation. ChR2 pos, ChAT-ChR2-YFP tracheas; ChR2 neg, littermates without the BAC transgene; paired t test.

(H) Experimental setup as in (G); independent experiment with tracheas with intact (+ Epith.) and with abraded (– Epith.) epithelium; paired t test.

(I) Increase in PTS 8 min after LED stimulation in tracheas from ChAT-ChR2-YFP mice (ChAT-ChR2 +) and controls (ChAT-ChR2 –). Whiskers show mean ± SEM, Mann-Whitney test.

(J) Cryosections of a formaldehyde-fixed ChAT-ChR2-YFP trachea, dorsal wall, depicting native ChR2-YFP expression (green) and antibody staining for YFP (yellow). Upper panel: a local ganglion with one nerve cell body is outlined (dotted line); arrowheads mark nerve fiber bundles. Lower panel: trachealis muscle with nerve fibers marked by arrowheads. Representative for five tracheas stained in two independent experiments.

See also Figure S5.

with the consequence of SP release and TACR1-driven activation of PTS could also potentially explain the effect evoked by fMet peptides. We tested this possibility by interfering at various levels in this chain of events (Figure S6B). However, neither inhibiting nAChR through the general antagonist mecamylamine nor blocking action potential generation with the voltage-gated sodium channel inhibitor tetrodotoxin nor TACR1 inhibition with RP67580 reduced the transport-stimulating effect of f-MKKFRW (Figures 6D and 6E). We then tested the impact of direct stimulation of such sensory nerve fibers on ciliary-driven transport.

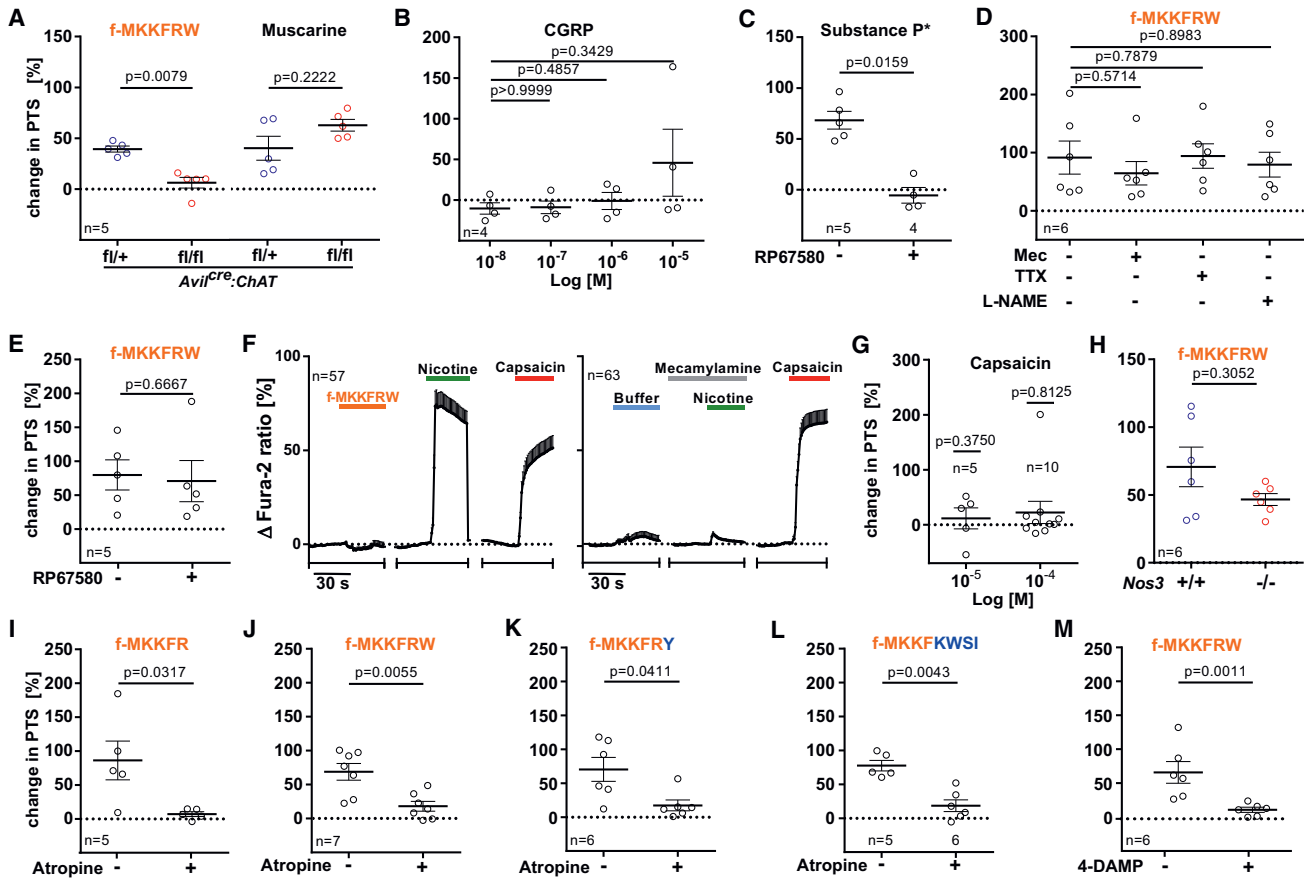

Figure 6. Increase of PTS upon Chemosensory Cell Stimulation Involves Neither Sensory Nerve Fibers nor Nitric Oxide, but Cholinergic Signaling through Muscarinic Receptors

(A–E and G–M) Explanted tracheas from mice with cell-type-specific deletion of ChAT (*Avil*^{cre}*:ChAT*$^{fl/fl}$) (A), genetic deletion of *Nos3* (H), and C57BL/6J mice (B–E, G, and I–M), increase in PTS measured 8 min after application of stimuli in the following concentrations (if not indicated in the figure): f-MKKFRW (A, D, E, H, and J) and all other fMet-peptides (I and K–M) (10 μM). Substance P* = stable substance P analog [Sar^{9}-Met(O$_2$)^{11}]-substance P (10 nM) (C). Inhibitors and their concentration were the TACR1 inhibitor RP67580 (10 μM) (E), the general nicotinic acetylcholine receptor inhibitor mecamylamine (Mec, 100 μM) (D), the inhibitor of voltage-gated sodium channels, tetrodotoxin (TTX, 1 μM) (D), the nitric oxide synthase inhibitor, L-NAME (20 μM) (D), the general muscarinic inhibitor atropine (1 μM) (I–L), and the muscarinic M3 receptor blocker, 4-DAMP (1 μM) (M). Whiskers show mean ± SEM; Mann-Whitney test.

(F) $[Ca^{2+}]_i$ in sensory *Chrna3-GFP*$^{+}$ neurons isolated from the jugular-nodose ganglion complex recorded as Fura-2 340/380 nm ratio; value immediately before stimulation was set as 100% and Δ upon stimulation depicted in percent. Concentrations were capsaicin (300 nM), mecamylamine (100 μM), nicotine (100 μM). *N*, number of neurons isolated from nine animals, data pooled from three independent experiments.

See also Figure S6.

First, we isolated sensory neurons expressing *chrna3* from the vagal jugular-nodose complex (Figure S6C), which gives rise to sensory tracheal innervation. Notably, these neurons were insensitive to direct application of f-MKKRW, but they responded to nicotine and the TRPV1 agonist capsaicin with a sharp increase in $[Ca^{2+}]_i$ (Figures 6F and S6C). In the explanted trachea, however, capsaicin did not elicit a significant acceleration of PTS (Figure 6G), consistent with a previous report showing an activating effect of capsaicin on mucociliary clearance only in presence of an intact vagus nerve and reflex loop (Bhashyam et al., 2010). From these experiments, we conclude that activation of sensory nerve terminals is not involved in accelerating clearance in response to f-MKKFRW.

We also tested whether endogenously produced NO could function as a potential mediator of enhanced ciliary activity upon exposure to bacterial products as suggested for mouse and human nasal epithelium (Carey et al., 2017; Lee et al., 2014). Consistent with a previous notion that the NO pathway in ciliated cells is activated by extracellular ATP (Gertsberg et al., 2004), the ATP response was reduced by 46% (Figure S6D) in tracheas with genetic deletion of endothelial NO synthase (*Nos3*), the NOS isoform linked to ciliary activation (Jiao et al., 2011). However, neither *Nos3* gene deficiency nor inhibition of NO synthesis by L-NAME had significant impact on the f-MKKFRW effect (Figures 6D and 6H).

By contrast, the general muscarinic inhibitor atropine almost fully eliminated the increase in PTS evoked by f-MKKFR, f-MKKFRW, f-MKKFRY, and f-MKKFKWSI (Figures 6I–6L). Notably, the cilio-activating effect of the *Pseudomonas* derived 3-oxo-C12-homoserine lactone, which persisted in absence of chemosensory cells (Figure 3J), was resistant to atropine (Figure S3J), similar to the small accelerating effect of 10 mM

denatonium (Figure S3F). Thus, this quorum-sensing molecule and the bacterial fMet peptides used here activated cilia-driven transport through independent mechanisms that must involve different cells and signaling pathways. We showed previously that genetic deletion of the receptor subtype M3, but not of others, abrogates muscarinic activation of PTS in the mouse trachea (Klein et al., 2009), and the M3 inhibitor 4-DAMP was as effective as atropine in suppressing the f-MKKFRW effect (Figure 6M). We therefore conclude that paracrine signaling from activated cholinergic chemosensory cells is independent of nerve fibers and operates through muscarinic M3 receptors.

Clearance-Accelerating Bacterial Peptides Occur Naturally

The data generated thus far demonstrate that synthetic fMet peptides corresponding in their sequence to the N termini of specific bacterial proteins drive ciliary activity through cholinergic chemosensory cells. We recently showed that f-MKKFRW can be detected by MALDI-TOF in supernatants of *E. coli* overexpressing MgrB (Bufe et al., 2019). Treatment with these supernatants resulted in increased PTS for up to 34% in a concentration-dependent manner (1:10–1:1,000 dilution), whereas supernatants from non-transfected bacteria with low basal expression of endogenous MgrB caused a small increase only at 1:10 dilution (Figure 7A). Importantly, this effect required the function of chemosensory cells, because it was lost in *Pou2f3*$^{-/-}$ tracheas (Figure 7B). Next, we collected sputum from six patients with chronic obstructive pulmonary disease (COPD) hospitalized because of acute exacerbation and presenting with pneumonia (Figure S7A). MALDI-TOF mass spectrometry identified the peptides f-MKKFR and f-MKKFRY in one and at least one of the unformylated hexapeptides MKKFRW and MKKFRY in each of the other patient samples (Figures 7C, S7A, and S7C). Protein-protein BLAST analyses revealed neither of these hexapeptides in human protein sequences, so they shall also derive from microbial origin. Unformylated MKKFRW, however, was not specific for patient sputum but was also detected in both saliva and induced sputum from four healthy volunteers, and f-MKKFRW was found in saliva, but not in induced sputum of one test person (Figures S7B and S7D). These findings in healthy persons are consistent with the abundant commensal occurrence of MgrB producers such as *E. coli* in the digestive tract, and it remains to be determined to which extent contamination with saliva may contribute to detection of unformylated MKKFRW in induced sputum. Thus, peptides with the cilio-activating signature can indeed be found under clinically relevant conditions.

Susceptibility to Tracheal Colonization by Pathogens Is Higher in Mice with a Defective Chemotransduction Signaling Pathway

As mucociliary clearance is one of the major innate defense mechanisms of the airways, we hypothesized that disruption of a pathway that links detection of virulence-associated bacterial peptides to activation of clearance might increase the risk of colonization or infection with naturally occurring pathogens. In mice, *B. pseudohinzii* is such a natural pathogen, primarily targeting the respiratory tract and the middle ear (Clark et al., 2016; Dewan et al., 2019; Ivanov et al., 2016; Perniss et al., 2018). The N terminus of its septation protein A, a transmembrane protein involved in cell division, starts with the MKKFR-related sequence MKKFLFD (UniProt *in silico* analysis). This recently identified *Bordetella* species has not yet found entry into the Federation for Laboratory Animal Science Associations (FELASA) recommendation list for the health monitoring of mouse colonies in experimental units and occurs widely spread, often unrecognized, in animal facilities (Hayashimoto et al., 2012; Ma et al., 2019). We recently reported an outbreak of *B. pseudohinzii* with tracheitis and bronchointerstitial pneumonia in one of our animal houses (Perniss et al., 2018). This outbreak also affected the colony of mice with targeted deletion of the *Trpm5* gene. While there was no obvious difference in the colonization of the pharynx with *B. pseudohinzii*, *Trpm5*$^{-/-}$ mice displayed a significantly higher *Bordetella* score in the trachea, and more animals presented with *B. pseudohinzii* progression into the lung compared to *Trpm5*$^{+/+}$ and *Trpm5*$^{+/-}$ mice kept in the same room (Figure 7D). Thus, mice with defective chemotransduction signaling present with a higher susceptibility of pathogen progression into the airways under conditions of natural exposure.

DISCUSSION

This study defines a subset of bacterial fMet peptides as powerful activators of an important defense mechanism in the airways, tracheal mucociliary clearance. Our work reveals a non-canonical signaling pathway for the detection of such peptides that is operated by cholinergic chemosensory cells in the mouse trachea, and we identify acetylcholine as an innate immune effector bypassing neural reflexes. Together, these results identify a cellular and molecular framework that defines how tracheal chemosensory cells integrate chemosensation of bacterial signals with innate defense.

Formylated bacterial signal peptides are N-terminal protein motifs that are now recognized as potent microorganism- and danger-associated molecular patterns in innate immunity. A broad range of such bacterial signal peptides can be recognized by Fpr1 and Fpr2, chemoattractant receptors expressed on leukocytes (Bufe et al., 2015; Bufe and Zufall, 2016; Weiß and Kretschmer, 2018). Most recently, we identified the core peptide motif f-MKKFRW as an activator of Fpr3 expressed by a subset of vomeronasal sensory neurons that mediate innate avoidance behavior (Bufe et al., 2019). The presently identified non-canonical pathway of formylated peptide detection by tracheal chemosensory cells differs markedly from those in leukocytes and vomeronasal neurons in the width of the spectrum of activating formylated peptides, in receptors, and in downstream intracellular signaling. Using a combination of genetic and pharmacological approaches, we found no evidence for an involvement of Fprs in peptide detection of tracheal chemosensory cells. The PLCβ2-IPTR3-TRPM5 signaling cascade identified here differs also markedly from the peptide signaling mechanisms of leukocytes, in which Fpr1 likely signals through TRPM2 (Qian et al., 2018; Wang et al., 2016), and of vomeronasal neurons, which employ the TPRC2 channel (Bufe et al., 2019) and in which ITPR3 is dispensable for sensory transduction (Chamero et al., 2017). In the trachea, we found a relatively narrow spectrum of peptide recognition with only six closely related agonists

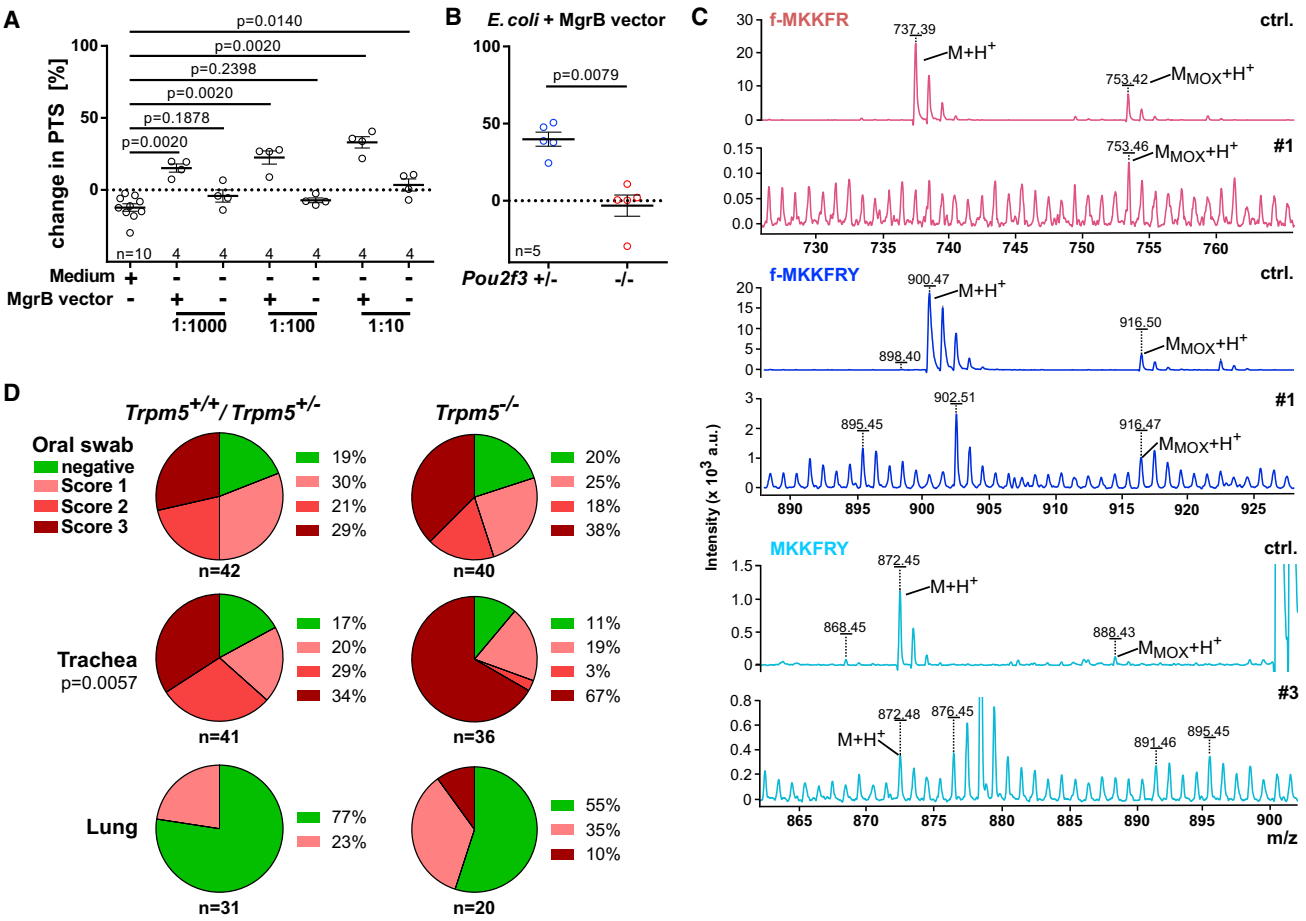

Figure 7. Bacteria Produce Clearance Accelerating Peptides and Infect Mice with a Defective Chemotransduction Signaling Pathway More Efficiently

(A) Supernatants from cultures of *E. coli* (1:10) overexpressing MgrB (vector p*mgrB-H6*) were applied to tracheas at three different dilutions; shown are changes in PTS after 8 min. Supernatants from non-transfected bacterial cultures and medium without bacteria served as controls. Whiskers show mean ± SEM, Mann-Whitney test.

(B) Supernatants from *E. coli* transfected with p*mgrB-H6* were applied to tracheas from *Pou2f3*$^{-/-}$ mice and their heterozygous littermates. Shown are changes in PTS 8 min after application. Whiskers show mean ± SEM, Mann-Whitney test.

(C) MALDI-TOF mass spectrometry of synthetic f-MKKFR (top), f-MKKFRY (3rd row) and MKKFRY (5th row), and sputa from patients hospitalized because of exacerbating COPD. Patient characteristics (#1–#6) are given in Figure S7A. Synthetic peptides exist in two forms: non-oxidized ($M+H^+$) and oxidized at the methionine ($M_{MOX}+H^+$). Peptides, either non-oxidized or oxidized, identified in patient sputa are indicated.

(D) Frequency of colonization with *B. pseudohinzii* in mice of different genotypes kept in the same room. Chi-square test.

See also Figure S7.

identified so far. Although five of them overlap with the set of Fpr3-activating peptides, removal of the C-terminal tryptophan (W) from the core motif f-MKKFRW caused complete loss of Fpr3 activation (Bufe et al., 2019), whereas the resulting pentapeptide f-MKKFR proved to be a strong activator of tracheal chemosensory cells driving ciliary activity. This pentapeptide sequence is most commonly conserved among respiratory pathogens. Our *in silico* analysis revealed its presence in 13 human pathogens that can cause bronchopulmonary infection, among which *S. pneumoniae* alone can be identified in 12%–85% of patients with community-acquired pneumonia in Europe (Torres et al., 2014). These 13 pathogenic species were found in 65%–69% of hospitalized patients with community-acquired pneumonia in Asian and European studies (Peto et al., 2014). Importantly, we identified this formylated pentapeptide and an extended variant in the sputum of a patient hospitalized because of exacerbating COPD with bronchopneumonia. We thus conclude that bacterial peptides with the f-MKKFR signature are naturally occurring, and monitoring their occurrence in the airway lining fluid may be well suited to assess the presence of the majority of bacterial respiratory pathogens.

The initial receptor recognizing these fMet peptides yet remains to be determined. The exclusive dependency on PLCβ2-IPTR3-TRPM5 signaling, i.e., the canonical taste transduction cascade, directed first attention toward taste receptors. Among them, sweet receptors appeared as prime candidates for sensing bacterial fMet peptides, since bacterial D-amino acids activate human heteromeric TAS1R2/3 sweet taste receptors

(Lee et al., 2017). However, our experiments ruled out both sweet and umami receptors as f-MKKFRW receptors, a result that was further supported by the fact that neither sweet nor umami receptor agonists mimicked the f-MKKFRW effect. Likewise, neither of our approaches supported a model in which Tas2r expressed by chemosensory cells drive mucociliary clearance in the mouse trachea. Similarly, the recently described cilioactivating effect of the *P. aeruginosa* quorum-sensing molecule *Pseudomonas* quinolone signal (PQS), an agonist at human TAS2Rs (Freund et al., 2018), was reduced only by 30% in *Trpm5*$^{-/-}$ tracheas (Hollenhorst et al., 2020), pointing to dominating direct effects on ciliated cells, as also reported for human airway cells (Freund et al., 2018). Notably, the full dependency on TRPM5 of the effect of f-MMKFR peptides observed in our study does not necessarily imply the involvement of taste receptors. TRPM5 is also critically involved in taste-receptor-independent mechanisms, such as triggering type 2 immune response in response to dietary and tritrichomonad-derived succinate through a succinate-receptor- and TRPM5-dependent pathway in intestinal tuft cells (Lei et al., 2018; Nadjsombati et al., 2018; Schneider et al., 2018). Collectively, our data show that tracheal chemosensory cells have evolved a mechanism for the detection of a bacterial fMet peptide signature that differs fundamentally from the mechanisms in the immune, accessory, olfactory, and oropharyngeal taste systems. We conclude that this pathway consists of a PLCβ2-ITPR3-Ca^{2+}-TRPM5-acetylcholine signaling cascade with a yet unknown receptor mechanism.

Cholinergic signaling by chemosensory cells has been primarily viewed in the context of fast signal transmission to nearby sensory nerve fibers expressing nAChR containing the α3 subunit. Upon stimulation, such sensory neurons trigger reflex responses that are suited to reduce further ingression or to facilitate expulsion of potentially harmful luminal content, such as slowing of breathing or flushing of the urethra by enhanced urinary bladder activity (Deckmann et al., 2014; Krasteva et al., 2011; Tizzano et al., 2010), and neurogenic inflammation (Saunders et al., 2014). The present data extend the functional spectrum of chemosensory cell-derived acetylcholine beyond these neurotransmitter-like actions. Triggered by bacterial fMet peptides with the f-MKKFR signature, acetylcholine serves as a nerve-independent but still acute activator of mucociliary clearance, a major innate defense mechanism of the lower airways. This activation of expulsion of luminal content synergizes with the neurally mediated inhibition of ingression through previously described respiratory reflexes (Krasteva et al., 2011; Tizzano et al., 2010), both mediated through acetylcholine.

Despite this synergy, stimuli that initiate the neural response are not identical to those activating clearance via chemosensory cells. Reported activators of the neural reflex are cycloheximide, denatonium, 3-oxo-C6-, and -C12-homoserine lactone (Hollenhorst et al., 2020; Krasteva et al., 2011, 2012; Tizzano et al., 2010). In the setup of the present study, they had highly diverse effects on mucosal PTS, ranging from inhibition (denatonium at 0.5 mM) over no effect (3-oxo-C6-homoserine lactone) to very minor (cycloheximide, denatonium at 10 mM) and distinct acceleration (3-oxo-C12-homoserine lactone). In neither case, however, did these effects require muscarinic signaling or the presence of chemosensory cells in our experiments. A recent study published during revision of this paper showed cholinergic signaling upon denatonium to a minor fraction of ciliated cells (16%), whereas calcium responses in the majority of ciliated cells was unaffected by cholinergic blockade (Hollenhorst et al., 2020). In accordance with this, direct, chemosensory cell-independent activation of ciliated cells by denatonium has previously been reported for the rat trachea (Lasconi et al., 2019) and cultured human lower-airway epithelia (Shah et al., 2009).

The combinatorial pattern of activation of chemosensory cells by f-MKKFR(W), cycloheximide, and denatonium in the calcium imaging experiments in tracheal whole mounts is complex. Thus, we currently cannot determine whether there are distinct subsets of chemosensory cells specifically connected to the neuronal reflex and paracrine pathway, respectively, or whether signaling pathways toward activation of sensory nerve fibers and ciliated cells are separated within the same chemosensory cell. This might involve basolateral acetylcholine release to address nAChR on sensory nerve terminals versus luminal release to address ciliated cells, similar to the luminal cholinergic signaling pathway regulating ion flux in ciliated cells through muscarinic M3 receptors that we described earlier (Hollenhorst et al., 2012).

These two avoidance responses, neuronal and ciliotropic, are not equally operative along the airway tree. Full closure of the airways, providing effective protection, e.g., against aspiration, can be achieved only at the larynx, which serves a gatekeeper function. In the nose, i.e., before incoming material has passed the larynx, virtually every cholinergic chemosensory cell is approached by trigeminal peptidergic sensory nerve fibers, and chemosensory cell activation by bacterial homoserine lactones results in initial respiratory arrest, followed by a marked decrease in respiratory rate (Tizzano et al., 2010). In the trachea, i.e., below the larynx, the presently recognized paracrine nerve-independent mechanism predominates, since here, only 6% of cholinergic chemosensory cells are in direct contact to peptidergic sensory nerve fibers (Krasteva et al., 2011). At this level, activation by bitter tastants and bacterial homoserine lactones leads to slowing of respiration through vagal afferents that is less marked than the trigeminal reflex evoked from the nose, and there is no transient respiratory arrest (Krasteva et al., 2011, 2012). Thus, the neural avoidance reflex restricting ingression can be particularly evoked before the gatekeeper, i.e., larynx, has been passed, whereas beyond that point, non-neuronal activation of an expulsion mechanism dominates.

If chemosensory cell-driven avoidance and expulsion mechanisms are of biological relevance, they should result in lower susceptibility to infection in the presence of pathogens. Indeed, lower airways of mice with defective chemosensory signal transduction (*Trpm5*$^{-/-}$) were more affected than their wild-type counterparts during a long-lasting outbreak of the murine respiratory pathogen *B. pseudohinzii* in the animal facility. While interpretation of this observation is somewhat limited by the fact that pathogen exposure was uncontrolled, this could also be considered as a strength, since this setting closely mimicked naturally occurring conditions. In line with this observation, a recent study demonstrated a novel population of chemosensory cells in the gingiva together with altered oral microbiota and exaggerated periodontitis in *Pou2f3*$^{-/-}$ and *Gnat3*$^{-/-}$ (= α-gustducin) mice (Zheng et al., 2019).

This higher susceptibility to infection and progression of disease may not exclusively depend on defective cholinergic

signaling, since acetylcholine is not the sole mediator produced by tracheal chemosensory cells. They abundantly express several interleukins (in particular IL-10, IL-18, and IL-25), CXCL12, and enzymes of the cysteinyl leukotriene synthesis pathway (Bankova et al., 2018; Montoro et al., 2018; von Moltke et al., 2016). Among these, IL-25 leads to a type 2 inflammation and stimulates chemosensory cell expansion within 3 days in response to common aeroallergens in a sequence of events that also involves cysteinyl leukotrienes (Bankova et al., 2018). Collectively, tracheal chemosensory cells appear to orchestrate various immune responses over a wide temporal range, covered by a spectrum of short- and long-acting mediators. The present data identify chemosensory cell-derived acetylcholine as an acute innate immune effector of the very early phase in response to the bacterial peptide signature f-MKKFR.

STAR★METHODS

Detailed methods are provided in the online version of this paper and include the following:

- KEY RESOURCES TABLE
- LEAD CONTACT AND MATERIALS AVAILABILITY
- EXPERIMENTAL MODEL AND SUBJECT DETAILS
  - Mice
  - Human samples
- METHOD DETAILS
  - Peptides
  - Bioinformatics
  - Measurement of particle transport speed
  - Measurement of ciliary beat frequency
  - Tissue fixation and immunofluorescence
  - X-gal staining
  - Cell sorting and RT-PCR
  - Transfection and calcium imaging in HEK Cells
  - Stimulation of tracheal acetylcholine release
  - Acetylcholine measurement by HPLC
  - Acetylcholine measurement with reporter cells
  - Ca^{2+}-Recording in sensory neurons
  - Ca^{2+} Imaging of $TRPM5^{+}$ cells in whole-mounts
  - Force recordings in organ bath
  - Bacterial supernatants
  - MALDI-TOF mass spectrometry of human samples
  - Bacteriological investigation of mouse colony
- QUANTIFICATION AND STATISTICAL ANALYSIS
- DATA AND CODE AVAILABILITY

SUPPLEMENTAL INFORMATION

Supplemental Information can be found online at https://doi.org/10.1016/j.immuni.2020.03.005.

ACKNOWLEDGMENTS

We thank T. Papadakis, M. Bodenbenner, S. Wiegand (Giessen), H. Lau (Frankfurt), and O. Maurer (Greifenstein) for excellent technical assistance; P. Schmidt (Giessen) for help with cell sorting and RT-PCR; G. Michel and the FACS core facility (Giessen) for help with cell sorting; and M. Pieper and P. König (University of Luebeck, Germany) for programming the MATLAB GUI to analyze ciliary beat frequency. For providing mice, we thank I. Matsumoto (Monell Chemical Senses Center, Philadelphia, PA, USA; $Pou2f3^{tm1Abek}$), R.F. Margolskee (Monell Chemical Senses Center; $Tg(Trpm5\text{-}EGFP)^{\#Sdmk}$), D. Wu (Yale University School of Medicine, USA; $PLC\beta2^{-/-}$), and A. Gödecke (Heinrich-Heine-University, Düsseldorf, Germany; $Nos3^{-/-}$), as well as W. Meyerhof (Saarland University) for all Tas2r plasmids. This work was supported by the German Research Foundation (DFG SFB-TR84, project A6 to W.K. and project B8 to T.H.; SFB-TR152, project 239283807 to V.C., T.G., T.L.-Z., U.B., and F.Z.; SFB 894, project A17 to F.Z. and T.L.-Z.; SFB1021, project Z02 to T.H.; and SCHU1259/10-1 to B.S.) and the German Center for Lung Research (DZL, ALI-1.1 to W.K. and FKZ 82DZL0003A4 and PH-2.7 to T.G.).

AUTHOR CONTRIBUTIONS

A.P. developed experimental protocols and conceived, designed, performed, and analyzed experiments. S.L. generated and initially characterized the $Tas2r^{-/-}$ mice. B. Boonen, M.K., A.-L.R., T.T., U.P., and L.D. performed and analyzed experiments. A.S., Ö.A., M.P., and K.D. contributed to the experiments. T.H., N.S., C.E., G.L., J.K., and T.L.-Z. designed and analyzed experiments. A.G. contributed human material, wrote ethics protocol, and diagnosed patients. V.C, T.G., J.O., and K.M. contributed materials and mouse strains. B.S. conceived, designed, and supervised experiments. S.O. designed and supervised generation of transgenic mice. S.K. and U.B. designed, generated, and initially characterized the TRPM5-IC/R26-DTA mice. F.Z. conceived, designed, and supervised experiments and provided conceptual input. B. Bufe conceived the study and designed and analyzed experiments. W.K. analyzed data and conceived and supervised the study. W.K., A.P., U.B., F.Z., and B. Bufe wrote the manuscript.

DECLARATION OF INTERESTS

The authors declare no competing interests.

SUPPORTING CITATIONS

The following references appear in the Supplemental Information: Chawla et al. (2014), Hartzell et al. (2007), Mcnulty et al. (2015), Singh et al. (2016), and Webley et al. (2009).

REFERENCES

Bailey, K.L., LeVan, T.D., Yanov, D.A., Pavlik, J.A., DeVasure, J.M., Sisson, J.H., and Wyatt, T.A. (2012). Non-typeable Haemophilus influenzae decreases cilia beating via protein kinase Cε. Respir. Res. *13*, 49.

Balentova, S., Conwell, S., and Myers, A.C. (2013). Neurotransmitters in parasympathetic ganglionic neurons and nerves in mouse lower airway smooth muscle. Respir. Physiol. Neurobiol. *189*, 195–202.

Bankova, L.G., Dwyer, D.F., Yoshimoto, E., Ualiyeva, S., McGinty, J.W., Raff, H., von Moltke, J., Kanaoka, Y., Frank Austen, K., and Barrett, N.A. (2018). The cysteinyl leukotriene 3 receptor regulates expansion of IL-25-producing airway brush cells leading to type 2 inflammation. Sci. Immunol. *3*, eaat9453.

Bhashyam, A.R., Mogayzel, P.J., Jr., Cleary, J.C., Undem, B.J., Kollarik, M., Fox, J., and Laube, B.L. (2010). Vagal control of mucociliary clearance in murine lungs: a study in a chronic preparation. Auton. Neurosci. *154*, 74–78.

Božičević, A., De Mieri, M., Nassenstein, C., Wiegand, S., and Hamburger, M. (2017). Secondary Metabolites in Allergic Plant Pollen Samples Modulate Afferent Neurons and Murine Tracheal Rings. J. Nat. Prod. *80*, 2953–2961.

Brockschnieder, D., Pechmann, Y., Sonnenberg-Riethmacher, E., and Riethmacher, D. (2006). An improved mouse line for Cre-induced cell ablation due to diphtheria toxin A, expressed from the Rosa26 locus. Genesis *44*, 322–327.

Bufe, B., and Zufall, F. (2016). The sensing of bacteria: emerging principles for the detection of signal sequences by formyl peptide receptors. Biomol. Concepts *7*, 205–214.

Bufe, B., Hofmann, T., Krautwurst, D., Raguse, J.-D., and Meyerhof, W. (2002). The human TAS2R16 receptor mediates bitter taste in response to beta-glucopyranosides. Nat. Genet. *32*, 397–401.

Bufe, B., Breslin, P.A.S., Kuhn, C., Reed, D.R., Tharp, C.D., Slack, J.P., Kim, U.-K., Drayna, D., and Meyerhof, W. (2005). The molecular basis of individual differences in phenylthiocarbamide and propylthiouracil bitterness perception. Curr. Biol. *15*, 322–327.

Bufe, B., Schumann, T., and Zufall, F. (2012). Formyl peptide receptors from immune and vomeronasal system exhibit distinct agonist properties. J. Biol. Chem. *287*, 33644–33655.

Bufe, B., Schumann, T., Kappl, R., Bogeski, I., Kummerow, C., Podgórska, M., Smola, S., Hoth, M., and Zufall, F. (2015). Recognition of bacterial signal peptides by mammalian formyl peptide receptors: a new mechanism for sensing pathogens. J. Biol. Chem. *290*, 7369–7387.

Bufe, B., Teuchert, Y., Schmid, A., Pyrski, M., Pérez-Gómez, A., Eisenbeis, J., Timm, T., Ishii, T., Lochnit, G., Bischoff, M., et al. (2019). Bacterial MgrB peptide activates chemoreceptor Fpr3 in mouse accessory olfactory system and drives avoidance behaviour. Nat. Commun. *10*, 4889.

Carey, R.M., Workman, A.D., Yan, C.H., Chen, B., Adappa, N.D., Palmer, J.N., Kennedy, D.W., Lee, R.J., and Cohen, N.A. (2017). Sinonasal T2R-mediated nitric oxide production in response to *Bacillus cereus*. Am. J. Rhinol. Allergy *31*, 211–215.

Chamero, P., Weiss, J., Alonso, M.T., Rodríguez-Prados, M., Hisatsune, C., Mikoshiba, K., Leinders-Zufall, T., and Zufall, F. (2017). Type 3 inositol 1,4,5-trisphosphate receptor is dispensable for sensory activation of the mammalian vomeronasal organ. Sci. Rep. *7*, 10260.

Chawla, K., Vishwanath, S., and Gupta, A. (2014). *Stenotrophomonas maltophilia* in Lower Respiratory Tract Infections. J. Clin. Diagn. Res. *8*, DC20–DC22.

Clapp, T.R., Medler, K.F., Damak, S., Margolskee, R.F., and Kinnamon, S.C. (2006). Mouse taste cells with G protein-coupled taste receptors lack voltage-gated calcium channels and SNAP-25. BMC Biol. *4*, 7.

Clark, S.E., Purcell, J.E., Sammani, S., Steffen, E.K., Crim, M.J., Livingston, R.S., Besch-Williford, C., and Fortman, J.D. (2016). *Bordetella pseudohinzii* as a Confounding Organism in Murine Models of Pulmonary Disease. Comp. Med. *66*, 361–366.

Cong, L., Ran, F.A., Cox, D., Lin, S., Barretto, R., Habib, N., Hsu, P.D., Wu, X., Jiang, W., Marraffini, L.A., and Zhang, F. (2013). Multiplex genome engineering using CRISPR/Cas systems. Science *339*, 819–823.

Deckmann, K., Filipski, K., Krasteva-Christ, G., Fronius, M., Althaus, M., Rafiq, A., Papadakis, T., Renno, L., Jurastow, I., Wessels, L., et al. (2014). Bitter triggers acetylcholine release from polymodal urethral chemosensory cells and bladder reflexes. Proc. Natl. Acad. Sci. USA *111*, 8287–8292.

Dewan, K.K., Taylor-Mulneix, D.L., Campos, L.L., Skarlupka, A.L., Wagner, S.M., Ryman, V.E., Gestal, M.C., Ma, L., Blas-Machado, U., Faddis, B.T., and Harvill, E.T. (2019). A model of chronic, transmissible Otitis Media in mice. PLoS Pathog. *15*, e1007696.

Dillon, W.C., Hampl, V., Shultz, P.J., Rubins, J.B., and Archer, S.L. (1996). Origins of breath nitric oxide in humans. Chest *110*, 930–938.

Eljamal, M., Wong, L.B., and Yeates, D.B. (1994). Capsaicin-activated bronchial- and alveolar-initiated pathways regulating tracheal ciliary beat frequency. J. Appl. Physiol. *77*, 1239–1245.

Frahm, S., Slimak, M.A., Ferrarese, L., Santos-Torres, J., Antolin-Fontes, B., Auer, S., Filkin, S., Pons, S., Fontaine, J.-F., Tsetlin, V., et al. (2011). Aversion to nicotine is regulated by the balanced activity of β4 and α5 nicotinic receptor subunits in the medial habenula. Neuron *70*, 522–535.

Freund, J.R., Mansfield, C.J., Doghramji, L.J., Adappa, N.D., Palmer, J.N., Kennedy, D.W., Reed, D.R., Jiang, P., and Lee, R.J. (2018). Activation of airway epithelial bitter taste receptors by *Pseudomonas aeruginosa* quinolones modulates calcium, cyclic-AMP, and nitric oxide signaling. J. Biol. Chem. *293*, 9824–9840.

Futatsugi, A., Nakamura, T., Yamada, M.K., Ebisui, E., Nakamura, K., Uchida, K., Kitaguchi, T., Takahashi-Iwanaga, H., Noda, T., Aruga, J., and Mikoshiba, K. (2005). IP3 receptor types 2 and 3 mediate exocrine secretion underlying energy metabolism. Science *309*, 2232–2234.

Gao, J.L., Lee, E.J., and Murphy, P.M. (1999). Impaired antibacterial host defense in mice lacking the N-formylpeptide receptor. J. Exp. Med. *189*, 657–662.

Gertsberg, I., Hellman, V., Fainshtein, M., Weil, S., Silberberg, S.D., Danilenko, M., and Priel, Z. (2004). Intracellular Ca^{2+} regulates the phosphorylation and the dephosphorylation of ciliary proteins via the NO pathway. J. Gen. Physiol. *124*, 527–540.

Gödecke, A., Decking, U.K., Ding, Z., Hirchenhain, J., Bidmon, H.J., Gödecke, S., and Schrader, J. (1998). Coronary hemodynamics in endothelial NO synthase knockout mice. Circ. Res. *82*, 186–194.

Gu, X., Karp, P.H., Brody, S.L., Pierce, R.A., Welsh, M.J., Holtzman, M.J., and Ben-Shahar, Y. (2014). Chemosensory functions for pulmonary neuroendocrine cells. Am. J. Respir. Cell Mol. Biol. *50*, 637–646.

Hartzell, J.D., Kim, A.S., Kortepeter, M.G., and Moran, K.A. (2007). *Acinetobacter pneumonia*: a review. MedGenMed *9*, 4.

Hayashimoto, N., Morita, H., Yasuda, M., Ishida, T., Kameda, S., Takakura, A., and Itoh, T. (2012). Prevalence of *Bordetella hinzii* in mice in experimental facilities in Japan. Res. Vet. Sci. *93*, 624–626.

Hofmann, T., Chubanov, V., Gudermann, T., and Montell, C. (2003). TRPM5 is a voltage-modulated and $Ca(^{2+})$-activated monovalent selective cation channel. Curr. Biol. *13*, 1153–1158.

Hollenhorst, M.I., Lips, K.S., Wolff, M., Wess, J., Gerbig, S., Takats, Z., Kummer, W., and Fronius, M. (2012). Luminal cholinergic signalling in airway lining fluid: a novel mechanism for activating chloride secretion via Ca^{2+}-dependent Cl^- and K^+ channels. Br. J. Pharmacol. *166*, 1388–1402.

Hollenhorst, M.I., Jurastow, I., Nandigama, R., Appenzeller, S., Li, L., Vogel, J., Wiederhold, S., Althaus, M., Empting, M., Altmüller, J., et al. (2020). Tracheal brush cells release acetylcholine in response to bitter tastants for paracrine and autocrine signaling. FASEB J. *34*, 316–332.

Ivanov, Y.V., Linz, B., Register, K.B., Newman, J.D., Taylor, D.L., Boschert, K.R., Le Guyon, S., Wilson, E.F., Brinkac, L.M., Sanka, R., et al. (2016). Identification and taxonomic characterization of *Bordetella pseudohinzii* sp. nov. isolated from laboratory-raised mice. Int. J. Syst. Evol. Microbiol. *66*, 5452–5459.

Jiang, H., Kuang, Y., Wu, Y., Xie, W., Simon, M.I., and Wu, D. (1997). Roles of phospholipase C β2 in chemoattractant-elicited responses. Proc. Natl. Acad. Sci. USA *94*, 7971–7975.

Jiao, J., Wang, H., Lou, W., Jin, S., Fan, E., Li, Y., Han, D., and Zhang, L. (2011). Regulation of ciliary beat frequency by the nitric oxide signaling pathway in mouse nasal and tracheal epithelial cells. Exp. Cell Res. *317*, 2548–2553.

Kaske, S., Krasteva, G., König, P., Kummer, W., Hofmann, T., Gudermann, T., and Chubanov, V. (2007). TRPM5, a taste-signaling transient receptor potential ion-channel, is a ubiquitous signaling component in chemosensory cells. BMC Neurosci. *8*, 49.

Kinnamon, S.C. (2012). Taste receptor signalling - from tongues to lungs. Acta Physiol. (Oxf.) *204*, 158–168.

Klein, M.K., Haberberger, R.V., Hartmann, P., Faulhammer, P., Lips, K.S., Krain, B., Wess, J., Kummer, W., and König, P. (2009). Muscarinic receptor subtypes in cilia-driven transport and airway epithelial development. Eur. Respir. J. *33*, 1113–1121.

Krasteva, G., Canning, B.J., Hartmann, P., Veres, T.Z., Papadakis, T., Mühlfeld, C., Schliecker, K., Tallini, Y.N., Braun, A., Hackstein, H., et al. (2011). Cholinergic chemosensory cells in the trachea regulate breathing. Proc. Natl. Acad. Sci. USA *108*, 9478–9483.

Krasteva, G., Canning, B.J., Papadakis, T., and Kummer, W. (2012). Cholinergic brush cells in the trachea mediate respiratory responses to quorum sensing molecules. Life Sci. *91*, 992–996.

Krasteva-Christ, G., Soultanova, A., Schütz, B., Papadakis, T., Weiss, C., Deckmann, K., Chubanov, V., Gudermann, T., Voigt, A., Meyerhof, W., et al.

(2015). Identification of cholinergic chemosensory cells in mouse tracheal and laryngeal glandular ducts. Int. Immunopharmacol. *29*, 158–165.

Kusumakshi, S., Voigt, A., Hübner, S., Hermans-Borgmeyer, I., Ortalli, A., Pyrski, M., Dörr, J., Zufall, F., Flockerzi, V., Meyerhof, W., et al. (2015). A Binary Genetic Approach to Characterize TRPM5 Cells in Mice. Chem. Senses *40*, 413–425.

Lakso, M., Pichel, J.G., Gorman, J.R., Sauer, B., Okamoto, Y., Lee, E., Alt, F.W., and Westphal, H. (1996). Efficient in vivo manipulation of mouse genomic sequences at the zygote stage. Proc. Natl. Acad. Sci. USA *93*, 5860–5865.

Lasconi, C., Pifferi, S., Hernandez-Clavijo, A., Merigo, F., Cecchini, M.P., Gonzalez-Velandia, K.Y., Agostinelli, E., Sbarbati, A., and Menini, A. (2019). Bitter tastants and artificial sweeteners activate a subset of epithelial cells in acute tissue slices of the rat trachea. Sci. Rep. *9*, 8834.

Lee, R.J., Xiong, G., Kofonow, J.M., Chen, B., Lysenko, A., Jiang, P., Abraham, V., Doghramji, L., Adappa, N.D., Palmer, J.N., et al. (2012). T2R38 taste receptor polymorphisms underlie susceptibility to upper respiratory infection. J. Clin. Invest. *122*, 4145–4159.

Lee, R.J., Chen, B., Redding, K.M., Margolskee, R.F., and Cohen, N.A. (2014). Mouse nasal epithelial innate immune responses to *Pseudomonas aeruginosa* quorum-sensing molecules require taste signaling components. Innate Immun. *20*, 606–617.

Lee, R.J., Hariri, B.M., McMahon, D.B., Chen, B., Doghramji, L., Adappa, N.D., Palmer, J.N., Kennedy, D.W., Jiang, P., Margolskee, R.F., et al. (2017). Bacterial d-amino acids suppress sinonasal innate immunity through sweet taste receptors in solitary chemosensory cells. Sci. Signal. *10*, eaam7703. 1.

Lei, W., Ren, W., Ohmoto, M., Urban, J.F., Jr., Matsumoto, I., Margolskee, R.F., and Jiang, P. (2018). Activation of intestinal tuft cell-expressed Sucnr1 triggers type 2 immunity in the mouse small intestine. Proc. Natl. Acad. Sci. USA *115*, 5552–5557.

Li, X., Staszewski, L., Xu, H., Durick, K., Zoller, M., and Adler, E. (2002). Human receptors for sweet and umami taste. Proc. Natl. Acad. Sci. USA *99*, 4692–4696.

Liberles, S.D., Horowitz, L.F., Kuang, D., Contos, J.J., Wilson, K.L., Siltberg-Liberles, J., Liberles, D.A., and Buck, L.B. (2009). Formyl peptide receptors are candidate chemosensory receptors in the vomeronasal organ. Proc. Natl. Acad. Sci. USA *106*, 9842–9847.

Lietsche, J., Imran, I., and Klein, J. (2016). Extracellular levels of ATP and acetylcholine during lithium-pilocarpine induced status epilepticus in rats. Neurosci. Lett. *611*, 69–73.

Liu, S., Lu, S., Xu, R., Atzberger, A., Günther, S., Wettschureck, N., and Offermanns, S. (2017). Members of Bitter Taste Receptor Cluster *Tas2r143/Tas2r135/Tas2r126* Are Expressed in the Epithelium of Murine Airways and Other Non-gustatory Tissues. Front. Physiol. *8*, 849.

Lossow, K., Hübner, S., Roudnitzky, N., Slack, J.P., Pollastro, F., Behrens, M., and Meyerhof, W. (2016). Comprehensive Analysis of Mouse Bitter Taste Receptors Reveals Different Molecular Receptive Ranges for Orthologous Receptors in Mice and Humans. J. Biol. Chem. *291*, 15358–15377.

Ma, L., Huang, S., Luo, Y., Min, F., He, L., Chen, M., Pan, J., Zhang, Y., and Wang, J. (2019). Isolation and characterization of *Bordetella pseudohinzii* in mice in China. Animal Model Exp. Med. *2*, 217–221.

Matsumoto, I., Ohmoto, M., Narukawa, M., Yoshihara, Y., and Abe, K. (2011). Skn-1a (Pou2f3) specifies taste receptor cell lineage. Nat. Neurosci. *14*, 685–687.

Mcnulty, M.C., Shibib, D.R., Steinbeck, J.L., Matushek, S., Pisano, J., Mullane, K., Beavis, K.G., Tesic, V., and Pitrak, D. (2015). *Bordetella bronchiseptica* Respiratory Infection Misdiagnosed as Pertussis by Multiplexed Nucleic Acid Test. Open Forum Infect. Dis. *2*, 1731.

Mercer, R.R., Russell, M.L., Roggli, V.L., and Crapo, J.D. (1994). Cell number and distribution in human and rat airways. Am. J. Respir. Cell Mol. Biol. *10*, 613–624.

Misgeld, T., Burgess, R.W., Lewis, R.M., Cunningham, J.M., Lichtman, J.W., and Sanes, J.R. (2002). Roles of neurotransmitter in synapse formation: development of neuromuscular junctions lacking choline acetyltransferase. Neuron *36*, 635–648.

Moine, F., Brechbühl, J., Nenniger Tosato, M., Beaumann, M., and Broillet, M.-C. (2018). Alarm pheromone and kairomone detection via bitter taste receptors in the mouse Grueneberg ganglion. BMC Biol. *16*, 12.

Montoro, D.T., Haber, A.L., Biton, M., Vinarsky, V., Lin, B., Birket, S.E., Yuan, F., Chen, S., Leung, H.M., Villoria, J., et al. (2018). A revised airway epithelial hierarchy includes CFTR-expressing ionocytes. Nature *560*, 319–324.

Nadjsombati, M.S., McGinty, J.W., Lyons-Cohen, M.R., Jaffe, J.B., DiPeso, L., Schneider, C., Miller, C.N., Pollack, J.L., Nagana Gowda, G.A., Fontana, M.F., et al. (2018). Detection of Succinate by Intestinal Tuft Cells Triggers a Type 2 Innate Immune Circuit. Immunity *49*, 33–41.e7.

Oliveira, M.J.R., Pereira, A.S., Guimarães, L., Grande, N.R., de Sá, C.M., and Aguas, A.P. (2003). Zonation of ciliated cells on the epithelium of the rat trachea. Hai *181*, 275–282.

Opremcak, L.B., and Rheins, M.S. (1983). Scanning electron microscopy of mouse ciliated oviduct and tracheal epithelium infected in vitro with *Bordetella pertussis*. Can. J. Microbiol. *29*, 415–420.

Pack, R.J., Al-Ugaily, L.H., and Morris, G. (1981). The cells of the tracheobronchial epithelium of the mouse: a quantitative light and electron microscope study. J. Anat. *132*, 71–84.

Perniss, A., Schmidt, N., Gurtner, C., Dietert, K., Schwengers, O., Weigel, M., Hempe, J., Ewers, C., Pfeil, U., Gärtner, U., et al. (2018). *Bordetella pseudohinzii* targets cilia and impairs tracheal cilia-driven transport in naturally acquired infection in mice. Sci. Rep. *8*, 5681.

Peto, L., Nadjm, B., Horby, P., Ngan, T.T.D., van Doorn, R., Van Kinh, N., and Wertheim, H.F.L. (2014). The bacterial aetiology of adult community-acquired pneumonia in Asia: a systematic review. Trans. R. Soc. Trop. Med. Hyg. *108*, 326–337.

Pyrski, M., Eckstein, E., Schmid, A., Bufe, B., Weiss, J., Chubanov, V., Boehm, U., and Zufall, F. (2017). Trpm5 expression in the olfactory epithelium. Mol. Cell. Neurosci. *80*, 75–88.

Qian, X., Zhao, H., Chen, X., and Li, J. (2018). Disruption of transient receptor potential melastatin 2 decreases elastase release and bacterial clearance in neutrophils. Innate Immun. *24*, 122–130.

Rivière, S., Challet, L., Fluegge, D., Spehr, M., and Rodriguez, I. (2009). Formyl peptide receptor-like proteins are a novel family of vomeronasal chemosensors. Nature *459*, 574–577.

Saunders, C.J., Christensen, M., Finger, T.E., and Tizzano, M. (2014). Cholinergic neurotransmission links solitary chemosensory cells to nasal inflammation. Proc. Natl. Acad. Sci. USA *111*, 6075–6080.

Schneider, C., O'Leary, C.E., von Moltke, J., Liang, H.-E., Ang, Q.Y., Turnbaugh, P.J., Radhakrishnan, S., Pellizzon, M., Ma, A., and Locksley, R.M. (2018). A Metabolite-Triggered Tuft Cell-ILC2 Circuit Drives Small Intestinal Remodeling. Cell *174*, 271–284.e14.

Sekiya, K., Futaesaku, Y., and Nakase, Y. (1989). Electron microscopic observations on ciliated epithelium of tracheal organ cultures infected with *Bordetella bronchiseptica*. Microbiol. Immunol. *33*, 111–121.

Shah, A.S., Ben-Shahar, Y., Moninger, T.O., Kline, J.N., and Welsh, M.J. (2009). Motile cilia of human airway epithelia are chemosensory. Science *325*, 1131–1134.

Shen, J.C., Cope, E., Chen, B., Leid, J.G., and Cohen, N.A. (2012). Regulation of murine sinonasal cilia function by microbial secreted factors. Int. Forum Allergy Rhinol. *2*, 104–110.

Singh, L., Cariappa, M.P., and Kaur, M. (2016). *Klebsiella oxytoca*: An emerging pathogen? Med. J. Armed Forces India *72* (*Suppl 1*), S59–S61.

Stempel, H., Jung, M., Pérez-Gómez, A., Leinders-Zufall, T., Zufall, F., and Bufe, B. (2016). Strain-specific Loss of Formyl Peptide Receptor 3 in the Murine Vomeronasal and Immune Systems. J. Biol. Chem. *291*, 9762–9775.

Stengel, P.W., Yamada, M., Wess, J., and Cohen, M.L. (2002). M(3)-receptor knockout mice: muscarinic receptor function in atria, stomach fundus, urinary bladder, and trachea. Am. J. Physiol. Regul. Integr. Comp. Physiol. *282*, R1443–R1449.

Tallini, Y.N., Shui, B., Greene, K.S., Deng, K.-Y., Doran, R., Fisher, P.J., Zipfel, W., and Kotlikoff, M.I. (2006). BAC transgenic mice express enhanced green

fluorescent protein in central and peripheral cholinergic neurons. Physiol. Genomics *27*, 391–397.

Tizzano, M., Gulbransen, B.D., Vandenbeuch, A., Clapp, T.R., Herman, J.P., Sibhatu, H.M., Churchill, M.E.A., Silver, W.L., Kinnamon, S.C., and Finger, T.E. (2010). Nasal chemosensory cells use bitter taste signaling to detect irritants and bacterial signals. Proc. Natl. Acad. Sci. USA *107*, 3210–3215.

Tizzano, M., Cristofoletti, M., Sbarbati, A., and Finger, T.E. (2011). Expression of taste receptors in solitary chemosensory cells of rodent airways. BMC Pulm. Med. *11*, 3.

Torres, A., Blasi, F., Peetermans, W.E., Viegi, G., and Welte, T. (2014). The aetiology and antibiotic management of community-acquired pneumonia in adults in Europe: a literature review. Eur. J. Clin. Microbiol. Infect. Dis. *33*, 1065–1079.

Trouillet, A.-C., Keller, M., Weiss, J., Leinders-Zufall, T., Birnbaumer, L., Zufall, F., and Chamero, P. (2019). Central role of G protein Gαi2 and Gαi2$^+$ vomeronasal neurons in balancing territorial and infant-directed aggression of male mice. Proc. Natl. Acad. Sci. USA *116*, 5135–5143.

Tsang, K.W., Leung, R., Fung, P.C.-W., Chan, S.L., Tipoe, G.L., Ooi, G.C., and Lam, W.K. (2002). Exhaled and sputum nitric oxide in bronchiectasis: correlation with clinical parameters. Chest *121*, 88–94.

von Moltke, J., Ji, M., Liang, H.-E., and Locksley, R.M. (2016). Tuft-cell-derived IL-25 regulates an intestinal ILC2-epithelial response circuit. Nature *529*, 221–225.

Wang, G., Cao, L., Liu, X., Sieracki, N.A., Di, A., Wen, X., Chen, Y., Taylor, S., Huang, X., Tiruppathi, C., et al. (2016). Oxidant Sensing by TRPM2 Inhibits Neutrophil Migration and Mitigates Inflammation. Dev. Cell *38*, 453–462.

Webley, W.C., Tilahun, Y., Lay, K., Patel, K., Stuart, E.S., Andrzejewski, C., and Salva, P.S. (2009). Occurrence of *Chlamydia trachomatis* and *Chlamydia pneumoniae* in paediatric respiratory infections. Eur. Respir. J. *33*, 360–367.

Weiß, E., and Kretschmer, D. (2018). Formyl-Peptide Receptors in Infection, Inflammation, and Cancer. Trends Immunol. *39*, 815–829.

Wijers, C.D., Chmiel, J.F., and Gaston, B.M. (2017). Bacterial infections in patients with primary ciliary dyskinesia: Comparison with cystic fibrosis. Chron. Respir. Dis. *14*, 392–406.

Yamashita, J., Ohmoto, M., Yamaguchi, T., Matsumoto, I., and Hirota, J. (2017). Skn-1a/Pou2f3 functions as a master regulator to generate Trpm5-expressing chemosensory cells in mice. PLoS ONE *12*, e0189340.

Yang, H., Wang, H., and Jaenisch, R. (2014). Generating genetically modified mice using CRISPR/Cas-mediated genome engineering. Nat. Protoc. *9*, 1956–1968.

Zhao, G.Q., Zhang, Y., Hoon, M.A., Chandrashekar, J., Erlenbach, I., Ryba, N.J.P., and Zuker, C.S. (2003). The receptors for mammalian sweet and umami taste. Cell *115*, 255–266.

Zhao, S., Ting, J.T., Atallah, H.E., Qiu, L., Tan, J., Gloss, B., Augustine, G.J., Deisseroth, K., Luo, M., Graybiel, A.M., and Feng, G. (2011). Cell type–specific channelrhodopsin-2 transgenic mice for optogenetic dissection of neural circuitry function. Nat. Methods *8*, 745–752.

Zheng, X., Tizzano, M., Redding, K., He, J., Peng, X., Jiang, P., Xu, X., Zhou, X., and Margolskee, R.F. (2019). Gingival solitary chemosensory cells are immune sentinels for periodontitis. Nat. Commun. *10*, 4496.

Zurborg, S., Piszczek, A., Martínez, C., Hublitz, P., Al Banchaabouchi, M., Moreira, P., Perlas, E., and Heppenstall, P.A. (2011). Generation and characterization of an Advillin-Cre driver mouse line. Mol. Pain *7*, 66.

STAR★METHODS

KEY RESOURCES TABLE

REAGENT or RESOURCE	SOURCE	IDENTIFIER
Antibodies		
Rabbit anti-TRPM5	Kaske et al., 2007	N/A
Goat anti-CGRP	Biotrend	Cat#BT17-2090-07; RRID: AB_2243858
Rabbit anti-Pou2f3	Sigma-Aldrich	Cat#HPA019652, RRID:AB_1855585
Chicken anti-GFP	Novus	Cat# NB100-1614, RRID:AB_10001164
Goat anti α-gustducin	Covalab	Cat#pab73402
Rabbit anti-DCLK1	abcam	Cat# ab31704, RRID:AB_873537
Rabbit anti-PLCβ2	Santa Cruz	Cat# sc-206, RRID:AB_632197
Goat anti-ChAT	Merck-Millipore	Cat# AB144P, RRID:AB_2079751
Rabbit anti-villin	US Biological	Cat# V2121-95, RRID:AB_2215974
Rabbit anti-α-gustducin	Santa Cruz	Cat# sc-395, RRID:AB_673678
Rat anti-CD45-APC-Vio770, clone 30F11	Miltenyi	Cat# 130-118-687, RRID:AB_2733121
Rat anti-CD326 (EpCAM)-VioBlue, clone caa7-9G8	Miltenyi	Cat# 130-102-421, RRID:AB_2657521
Donkey IgG anti-chicken IgY (H+L), FITC-conjugate	Dianova	Cat# 703-095-155, RRID:AB_2340356
Donkey anti-rabbit IgG (H+L) secondary antibody, Alexa Fluor 488-conjugate	Thermo Fisher	Cat# A-21206, RRID:AB_2535792
Donkey anti-rabbit IgG, Cy3-conjugate	Merck Millipore	Cat# AP182C, RRID:AB_92588
Donkey IgG anti-rabbit IgG (H+L), Cy5-conjugate	Dianova	Cat# 711-175-152, RRID:AB_2340607
Donkey anti-goat IgG, Cy3-conjugate	Merck Millipore	Cat# AP180C, RRID:AB_92570
Donkey anti-goat IgG (H+L) secondary antibody, Alexa Fluor 488-conjugate	Thermo Fisher	Cat# A-11055, RRID:AB_2534102
Bacterial and Virus Strains		
E. coli BL21 (DE3)	New England BioLabs	Cat#C2527
Chemicals, Peptides, and Recombinant Proteins		
Adenosine 5′-triphosphate di(tris) salt hydrate (ATP)	Sigma Aldrich	Cat#A9062
Papain	Sigma Aldrich	Cat#P4762
Laminin	Thermo Fisher	Cat#23017015
Leupeptin	Sigma Aldrich	Cat#62070
Poly-L-lysine	Sigma Aldrich	Cat#P-5899
L-Cysteine	Sigma Aldrich	Cat#14495
t-Boc2	Bachem	Cat#4003823
Cyclosporin H	Santa Cruz	Cat#Sc-203013
Mecamylamine	Sigma Aldrich	Cat#M9020
TTX (Tetrodotoxin citrate)	BioTrend	Cat#BN0518
L-NAME (N omega-Nitro-L-arginine methyl ester hydrochloride)	ENZO	Cat#ALX-105-003G005
Atropine	Sigma Aldrich	Cat#A0257
Sputasol	Thermo Fisher	Cat#SR0233A
Eserine	Sigma Aldrich	Cat#E-805
4-DAMP(1,1-Dimethyl-4-diphenylacetoxypiperidinium iodide)	Sigma Aldrich	Cat#SML0255
Fura-2-AM	Thermo Fisher	Cat#F1221
Bacitracin	Carl Roth	Cat#5655.2
Neomycin trisulfate salt hydrate	Sigma Aldrich	Cat#N6386
Cephalexin hydrate	Sigma Aldrich	Cat#C4895

(*Continued on next page*)

Continued

REAGENT or RESOURCE	SOURCE	IDENTIFIER
Brain heart infusion broth	Thermo Fisher	Cat#CM1135
Penicillin-Streptomycin	Sigma Aldrich	Cat#P4333
Blood agar plate	Oxoid	Cat#CM0055
L-15 Medium	Thermo Fisher	Cat#11415056
Propidium iodide	Tonbo Biosciences	Cat#13-6990-T200
Fluo-4-AM	Thermo Fisher	Cat#F14201
Isopropyl β-D-1-thiogalactopyranoside	Sigma Aldrich	Cat#I6758
MEM Non-Essential Amino Acids Solution	Thermo Fisher	Cat#11140050
M9 Minimal Salts	Thermo Fisher	Cat#A1374401
MEM Amino Acids (50x) solution	Sigma Aldrich	Cat#M5550
M9 Minimal Salts, 5x	Sigma Aldrich	Cat#M6030
Capsaicin	Sigma Aldrich	Cat#211275
MACSQuant Running Buffer	Miltenyi Biotec	Cat#130-092-747
RP 67580	Tocris Bioscience	Cat#1635
[Sar^9, $Met(O_2)^{11}$]-Substance P	Sigma Aldrich	Cat#S3672
Calcitonin Gene-Related Peptide (CGRP)	Sigma Aldrich	Cat#C0292
N-(β-Ketocaproyl)-L-homoserine lactone (3-O-C6-(L)-HSL)	Cayman CHEMICAL	Cat#10011207
N-(3-Oxododecanoyl)-L-homoserine lactone (3-Oxo-C12-HSL)	Sigma Aldrich	Cat#O9139
Allylisothiocyanate	Sigma Aldrich	Cat#36682
Dimethylformamide	Sigma Aldrich	Cat#PHR1553-3X
5-Bromo-4-chloro-3-indolyl-β-D-galactopyranoside (X-Gal)	Sigma Aldrich	Cat#B4252
Denatonium benzoate	Sigma Aldrich	Cat#D5765
2-Propyl thietane (2-PT)	AKos Consulting	Cat#AKOS023876051
Cycloheximide	Sigma Aldrich	Cat#C7698
Quinine	Sigma Aldrich	Cat#145904
Arbutin	Sigma Aldrich	Cat#A4256
5-Propyl-2-thiouracil (5-PTU)	Sigma Aldrich	Cat#P0643
6-Propyl-2-thiouracil (6-PTU)	Sigma Aldrich	Cat#P3755
Muscarine chloride	Sigma Aldrich	Cat#M104
L-Glutamic acid monosodium salt monohydrate	Sigma Aldrich	Cat#49621
Sucrose	Sigma Aldrich	Cat#84097
Phenylbutazone	Sigma Aldrich	Cat#P8386
Sucralose	Sigma Aldrich	Cat#69293
DMEM, high glucose	Sigma Aldrich	Cat#6429
dNTP Set	QIAGEN	Cat#201900
AmpliTaq Gold	Applied Biosystems	Cat#N8080247
Critical Commercial Assays		
CloneJET PCR Cloning Kit	Thermo Fisher	Cat#K1231
mMESSAGE mMACHINE T7 ULTRA Transcription Kit	Thermo Fisher	Cat#AM1345
MEGAshortscript T7 Transcription Kit	Thermo Fisher	Cat#AM1354
MEGAclear Transcription Clean-Up Kit	Thermo Fisher	Cat#AM1908
SuperScriptIII CellsDirect cDNA Synthesis System	Invitrogen	Cat#18080-200
RNeasy Mini Kit	QIAGEN	Cat#74104
Pure Yield Plasmid Midiprep System	Promega	Cat#A2495
jetPEI	Polyplus transfection	Cat#101-10N

(*Continued on next page*)

Continued

REAGENT or RESOURCE	SOURCE	IDENTIFIER
Experimental Models: Cell Lines		
M3WT4 (CHO-K1 cells expressing rat M3 muscarinic acetylcholine receptor)	ATCC	Cat#CRL-1981
HEK293T	DSMZ	Cat# ACC-635
Biological Samples		
Sputum samples of 6 hospitalized COPD patients	See Method Details	N/A
Saliva and sputum samples of 6 volunteers	See Method Details	N/A
Experimental Models: Organisms/Strains		
Mouse: C57BL/6JRj	Janvier Labs	MGI Cat#5751862, RRID:MGI:5752053
Mouse: FVB/NCrl	Charles River	IMSR Cat# CRL:207, RRID:IMSR_CRL:207
Mouse: Tg(Trpm5-EGFP)#Sdmk (TRPM5-GFP)	Clapp et al., 2006	N/A
Mouse: B6.Cg-Tg(RP23-268L19-EGFP)2Mik/J (ChAT-eGFP)	The Jackson Laboratory	IMSR Cat# JAX:007902, RRID: IMSR_JAX:007902
Mouse: B6.Cg-Tg(Chat-COP4*H134R/EYFP,Slc18a3) 6Gfng/J (ChAT-ChR2-YFP)	The Jackson Laboratory	IMSR Cat# JAX:014546, RRID: IMSR_JAX:014546
Mouse: B6.129P2-Trpm5^{tm1Dgen}/J (TRPM5$^{-/-}$)	The Jackson Laboratory	IMSR Cat# JAX:005848, RRID: IMSR_JAX:005848
Mouse: PLCβ2$^{-/-}$	Jiang et al., 1997	N/A
Mouse: B6.(Tas2r143-Tas2r135-Tas2r126)<^{tm}> (Tas2r$^{-/-}$)	This paper	N/A
Mouse: IP3R3$^{-/-}$	Futatsugi et al., 2005	N/A
Mouse: Pou2f3^{tm1Abek} (Pou2f3$^{-/-}$)	Matsumoto et al., 2011	N/A
Mouse: TRPM5-IRES-Cre	Kusumakshi et al., 2015	N/A
Mouse: R26:lacZbpA^{flox}DTA	Brockschnieder et al., 2006	N/A
Mouse: TRPM5-IRES-Cre-R26:lacZbpA^{flox}DTA (TRPM5-DTA)	This paper	N/A
Mouse: B6;129S-Gt(ROSA)$^{26Sortm95.1(CAG-GCaMP6f)Hze}$/J	Jackson Laboratory	IMSR Cat# JAX:024105, RRID: IMSR_JAX:024105
Mouse: TRPM5-ires-Cre-B6;129S-Gt (ROSA)$^{26Sortm95.1(CAG-GCaMP6f)Hze}$/J	This paper	N/A
Mouse: C57BL/6NTac-Fpr1^{Tm1Gao}N6 (Fpr1$^{-/-}$)	Gao et al., 1999	N/A
Mouse: Fpr3$^{tm1b(EUCOMM)Hmgu}$ (Fpr3$^{-/-}$)	Bufe et al., 2019	MGI Cat#5584405
Mouse: B6;129-Chat^{tm1Jrs}/J (Chat^{flox})	The Jackson Laboratory Misgeld et al., 2002	IMSR Cat# JAX:016920, RRID:IMSR_JAX:016920
Mouse: B6;D2-Tg(Avil-cre)1Phep/Cnrm (Avil^{cre})	EMMA Mouse Repository Zurborg et al., 2011	IMSR Cat# EM:05542, RRID:IMSR_EM:05542
Mouse: B6;129-Chat^{tm1Jrs}/J-B6;D2-Tg(Avil-cre) 1Phep/Cnrm (Avil^{cre}:Chat$^{fl/fl}$)	This paper	N/A
Mouse: Chrna3-eGFP	Frahm et al., 2011	N/A
Mouse: C57BL/6.129/Ola-eNOS^{tm} (Nos3$^{-/-}$)	Gödecke et al., 1998	N/A
Mouse: B6;129-Tas1r3tm1Csz/J (Tas1r3$^{-/-}$)	The Jackson Laboratory	IMSR Cat# JAX:013066, RRID:IMSR_JAX:013066
Oligonucleotides		
Left **loxP sgRNA** 5′-CAGTTGGTTAGTCCTATAAGAGG-3′	This Paper	N/A
Right **loxP sgRNA** 5′-GTGGCTTTGTAGCGTATACCTGG-3′	This Paper	N/A
Left **loxP single-stranded DNA donor** 5′-AAGAAATCC CTACTGCATAACAAGTCTCAAATCCAGTCAGAAAACAG TTGGTTAGTCCTA**ataacttcgtatagcatacattatacgaagttat (loxP)** Gctagc (Nhel) TAAGAGGCATATCTCTAATACAC TAGTGGCCACATCTTGACTGGCAAACACATTGCTTCA-3‘	This Paper	N/A

(*Continued on next page*)

Continued

REAGENT or RESOURCE	SOURCE	IDENTIFIER
Right **loxP single-stranded DNA donor** 5′-TAAGT CTTTTTCTGAATGAAAGATAATGTTTATTCAATGC AGAAGTGGCTTTGTAGCGTA**ataacttcgtatagcatac attatacgaagttat (loxP)** Gaattc (EcoRI) TACCTGGG GAAGTAAAAGGGTTCCCAAAGACAGGAAAATGA GGATTGGTCTTATTTATTT-3′	This Paper	N/A
right ***loxP*** site for genotyping Tas2r KO: (P3) 5′-GACCAATCCTCATTTTCCTGTC-3′, (P4) 5′-CCAAGAGCTCTTTGTTCTGTCT-3′	This Paper	N/A
left ***loxP*** site for genotyping Tas2r KO: (P1) 5′-GAAGACAGCTACACTGTACTCA-3′, (P2) 5′-CAGGTTAACAGAAGCAGGCAA-3′	This Paper	N/A
RT-PCR primer are listed in Table S6	This Paper	N/A
Recombinant DNA		
pX330-U6-Chimeric_BB-CBh-hSpCas9	Addgene	Cat#42230
pJET1.2/blunt	Thermo Fisher	Cat#K1231
mTas2r102 in PEAK 10	Lossow et al., 2016	N/A
mTas2r103 in PEAK 10	Lossow et al., 2016	N/A
mTas2r104 in PEAK 10	Lossow et al., 2016	N/A
mTas2r105 in pCDNA5_FRT	Lossow et al., 2016	N/A
mTas2r106 in PEAK 10	Lossow et al., 2016	N/A
mTas2r107 in PEAK 10	Lossow et al., 2016	N/A
mTas2r108 in PEAK 10	Lossow et al., 2016	N/A
mTas2r109 in PEAK 10	Lossow et al., 2016	N/A
mTas2r110 in PEAK 10	Lossow et al., 2016	N/A
mTas2r115 in PEAK 10	Lossow et al., 2016	N/A
mTas2r117 in PEAK 10	Lossow et al., 2016	N/A
mTas2r118 in PEAK 10	Lossow et al., 2016	N/A
mTas2r119 in pCDNA5_FRT	Lossow et al., 2016	N/A
mTas2r120 in PEAK 10	Lossow et al., 2016	N/A
mTas2r121 in PEAK 10	Lossow et al., 2016	N/A
mTas2r122 in PEAK 10	Lossow et al., 2016	N/A
mTas2r123 in PEAK 10	Lossow et al., 2016	N/A
mTas2r124 in PEAK 10	Lossow et al., 2016	N/A
mTas2r125 in PEAK 10	Lossow et al., 2016	N/A
mTas2r126 in PEAK 10	Lossow et al., 2016	N/A
mTas2r129 in PEAK 10	Lossow et al., 2016	N/A
mTas2r130 in PEAK 10	Lossow et al., 2016	N/A
mTas2r131 in PEAK 10	Lossow et al., 2016	N/A
mTas2r134 in PEAK 10	Lossow et al., 2016	N/A
mTas2r135 in PEAK 10	Lossow et al., 2016	N/A
mTas2r136 in PEAK 10	Lossow et al., 2016	N/A
mTas2r137 in PEAK 10	Lossow et al., 2016	N/A
mTas2r138 in pCDNA5_FRT	Lossow et al., 2016	N/A
mTas2r139 in PEAK 10	Lossow et al., 2016	N/A
mTas2r140 in PEAK 10	Lossow et al., 2016	N/A
mTas2r143 in pCDNA5_FRT	Lossow et al., 2016	N/A
mTas2r144 in pCDNA5_FRT	Lossow et al., 2016	N/A
mTas2r114 in PEAK 10	Lossow et al., 2016	N/A
mTas2r113 in PEAK 10	Lossow et al., 2016	N/A

(*Continued on next page*)

Continued		
REAGENT or RESOURCE	SOURCE	IDENTIFIER
G16-Gust44 in pCDNA3	Bufe et al., 2005	N/A
G16 in pCIS	Bufe et al., 2002	N/A
mFpr1 in pCDNA3	Bufe et al., 2012	N/A
mFpr2 in pCDNA3	Bufe et al., 2012	N/A
mFpr3 in pCDNA3	Bufe et al., 2012	N/A
mFpr-rs3 in pCDNA3	Bufe et al., 2012	N/A
mFpr-rs4 in pCDNA3	Bufe et al., 2012	N/A
mFpr-rs6 in pCDNA3	Bufe et al., 2012	N/A
mFpr-rs7 in pCDNA3	Bufe et al., 2012	N/A
pmgrB-H6	Bufe et al., 2019	N/A
Software and Algorithms		
GraphPrism 7	GraphPad Software	https://www.graphpad.com/scientific-software/prism/
MATLABR2016b	MathWorks	https://www.mathworks.com/products/new_products/release2016b.html
ImageJ 1.49	NIH	https://imagej.nih.gov/ij/
Image Pro Analyzer 6.2	Media Cybernetics	http://www.mediacy.com/imageproplus
Inkscape version 0.92.3	Inkscape community	https://inkscape.org/
LabChart 6	ADInstruments	https://www.adinstruments.com/products/labchart
BD FACSDIVA SOFTWARE V6.1.3	BD Biosciences	http://www.bdbiosciences.com/us/instruments/research/software/flow-cytometry-acquisition/bd-facsdiva-software/m/111112/overview
ZEN 2010B SP1		https://www.zeiss.de/mikroskopie/downloads/zen.html
Compass 1.3 software package (FlexControl 2.4, FlexAnalysis 3.0, BioTools 3.0)	Bruker Daltonics	https://www.bruker.com/
Biotyper V3.3.1.0	Bruker Daltonics	https://www.bruker.com/
FLOWJO v10.6.1	BD Biosciences	https://www.flowjo.com/solutions/flowjo
LAS X Life science 1.10.12420	Leica	https://www.leica-microsystems.com/de/produkte/mikroskop-software/
Adobe Illustrator	Adobe	N/A
Prizmatix pulser software V.2.3.1	Prizmatix	https://www.prizmatix.com/software.htm
Igor Pro 6.12	Wavemetrics	https://www.wavemetrics.com/
Origin 7.5	OriginLab	https://www.originlab.com/
Other		
Dynabeads Protein G	Invitrogen	Cat#10003D
Fetal Bovine Serum	Thermo Fisher	Cat#26140079
Cell Strainer 70 μM	Sigma Aldrich	Cat#CLS431751

LEAD CONTACT AND MATERIALS AVAILABILITY

Further information and requests for resources and reagents should be directed to and will be fulfilled by the Lead Contact, Wolfgang Kummer (wolfgang.kummer@anatomie.med.uni-giessen.de). The B6.(Tas2r143-Tas2r135-Tas2r126)<^{tm}> (Tas2r$^{-/-}$) mouse line is available from Stefan Offermanns (MPI for Heart and Lung Research, Bad Nauheim, Germany) with a completed Materials Transfer Agreement. The TRPM5-IRES-Cre-B6 and TRPM5-IRES-Cre-R26:lacZbpA^{flox}DTA (TRPM5-DTA) mouse lines generated in this study will be made available on request by Ulrich Boehm (Saarland University, Homburg, Germany), but we may require a payment and/or a completed Materials Transfer Agreement if there is potential for commercial application. There are restrictions to the availability of *Avil^{cre}:Chat$^{fl/fl}$* mice due to third party use restrictions made by the distributors of strains used for crossbreeding.

EXPERIMENTAL MODEL AND SUBJECT DETAILS

Mice

Mice older than 8 weeks were used throughout. Mice were age-matched within each experiment, but pooled results include both male and female mice of varying ages. All animals were housed under standard laboratory SPF conditions (10 h dark, 14 h light), with free access to food and water. All animals were held according to the European Community guidelines for the care and use of animals. Breeding and use of samples of scarified mice for further *in vitro* experiments were registered by the responsible authorities at the Regierungspräsidium Giessen (Hesse), Darmstadt (Hesse), Saarbrücken (Saarland), and Bezirksregierung Düsseldorf, Germany. In this study, 22 different mouse strains or crosses were used. C57BL/6JRj mice were purchased from Janvier Labs. A mouse line carrying a constitutive null mutation in *Trpm5* (*Trpm5*^{tm1Dgen}, 129P2/OlaHsd) was obtained from Jackson laboratory (Stock No. 005848) and backcrossed (six generations) on to the C57BL/6J background. B6.Cg-Tg(Chat-COP4*H134R/EYFP,Slc18a3)6Gfng/J (ChAT-ChR2-YFP), B6.Cg-Tg(RP23-268L19-EGFP)2Mik/J (*Chat*-eGFP), B6;129-Chat^{tm1Jrs}/J (*Chat*^{fl}), B6;129S-Gt(ROSA)26Sor$^{tm95.1(CAG-GCaMP6f)Hze}$/J and B6;129-Tas1r3tm1Csz/J (*Tas1r3*$^{-/-}$) mice were purchased from Jackson Laboratories. FVB/NCrl mice were purchased from Charles River. The following mouse strains have been characterized previously: Pou2f3^{tm1Abek} (*Pou2f3*$^{-/-}$) mice (Matsumoto et al., 2011), Tg(Trpm5-EGFP)#Sdmk (*Trpm5*-GFP) mice (Clapp et al., 2006), *PLCβ2*$^{-/-}$ mice (Jiang et al., 1997), *Itpr3*$^{-/-}$ mice (Futatsugi et al., 2005), C57BL/6NTac-Fpr1^{Tm1Gao}N6 (*Fpr1*$^{-/-}$) mice (Gao et al., 1999), Fpr3$^{tm1b(EUCOMM)Hmgu}$ (*Fpr3*$^{-/-}$) mice (Bufe et al., 2019), B6;D2-Tg(Avil-cre)1Phep/Cnrm (*Avil*^{cre}) mice (Zurborg et al., 2011), *Chrna3*-eGFP mice (Frahm et al., 2011), C57BL/6.129/Ola-eNOS^{tm} (*Nos3*$^{-/-}$) mice (Gödecke et al., 1998). To generate B6.(Tas2r143-Tas2r135-Tas2r126)<tm> mice (*Tas2r*$^{-/-}$), a 38.1 kb region on mouse chromosome 6 which carries the genes Tas2r143, Tas2r135 and Tas2r126 was flanked by loxP sites using CRISPR/Cas technology (Yang et al., 2014). Briefly, the DNA encoding Cas9 from the px330 vector (Addgene) (Cong et al., 2013) was amplified by PCR and inserted into the pJET1.2/blunt cloning vector (CloneJET PCR Cloning Kit, Thermo Scientific). This plasmid was linearized, digested by XbaI and used as a template for *in vitro* transcription using mMESSAGE mMACHINE T7 ULTRA kit (Life Technologies) to generate Cas9 mRNA. Two sgRNAs were designed to guide Cas9 to the insertion sites of the left and right *loxP* sites, which were 2153 base pairs upstream of the Tas2r143 start codon and 724 base pairs downstream of the Tas2r126 stop codon. Single-stranded DNA, which are reverse complementary to the sequences of sgRNAs, were synthesized (Sigma-Aldrich), annealed with a T7 promoter oligo at 5′ and used as a template for *in vitro* transcription using MEGAshortscript T7 kit (Life Technologies) to generate sgRNAs. Both the Cas9 mRNA and the sgRNAs were purified using MEGAclear kit (Life Technologies) and eluted in RNase-free water. Single-stranded DNA donors containing the *loxP* site and a restriction site flanked by 60 bp homologous arms on each side adjoining the DNA double-strand breaks were designed and synthesized by Sigma-Aldrich. Zygote injection was performed as described (Yang et al., 2014). Of 109 pups born, 1 pup was found to carry the *loxP* sites at the correct position as determined by PCR and sequencing. The *Tas2r143*/*Tas2r135*/*Tas2r126*-floxed mice were mated to the *EIIa-Cre* mice (Lakso et al., 1996) to generate *Tas2r143*/*Tas2r135*/*Tas2r126* triple knockout mice by recombining *loxP* sites in the early embryonic stage. The left *loxP* site was genotyped by PCR using forward primer P1 (5′-GAAGACAGCTACACTGTACTCA-3′) and reverse primer P2 (5′-CAGGTTAACAGAAGCAGGCAA-3′), amplifying a 219 bp and a 308 bp fragment for the wild-type and the floxed alleles, respectively. The right *loxP* site was genotyped by PCR using forward primer P3 (5′-GACCAATCCTCATTTTCCTGTC-3′) and reverse primer P4 (5′-CCAAGAGCTCTTTGTTCTGTCT-3′), amplifying a 324 bp and a 404 bp fragment for the wild-type and the floxed alleles, respectively. The genotype of *Tas2r143*/*Tas2r135*/*Tas2r126* triple knock-out mice was analyzed by PCR using primers P1/P2, giving a 219 bp fragment for the wild-type allele, and P1/4, giving a 443 bp fragment for the null allele. Furthermore, absence of *Tas2r143*/*Tas2r135*/*Tas2r126* mRNA in tongue was confirmed by RT-PCR (Figure S3A). Mice were backcrossed with C57BL/6J mice for at least 6 generations. To generate TRPM5-IRES-Cre-R26:lacZbpA^{flox}DTA (TRPM5-DTA) mice, the strains TRPM5-IRES-Cre (Kusumakshi et al., 2015) and R26:lacZbpAfloxDTA (Brockschnieder et al., 2006) were cross-bred. Absence of cholinergic chemosensory cells in the trachea was confirmed by immunostaining (Figure 2G). To generate B6;129-Chat^{tm1Jrs}/J-B6;D2-Tg(Avil-cre)1Phep/Cnrm (*Avil*^{cre}*:Chat*$^{fl/fl}$) mice, the strains B6;129-Chat^{tm1Jrs} (Misgeld et al., 2002) and B6;D2-Tg(Avil-cre)1Phep/Cnrm (Zurborg et al., 2011) were cross-bred. To generate TRPM5-IRES-Cre-B6;129S-Gt(ROSA)26Sor$^{tm95.1(CAG-GCaMP6f)Hze}$/J mice, the strains TRPM5-IRES-Cre (Kusumakshi et al., 2015) and B6;129S-Gt(ROSA)26Sor$^{tm95.1(CAG-GCaMP6f)Hze}$/J were cross-bred. To produce experimental animals heterozygous for TRPM5, Cre, and GCaMP6f (*Trpm5*$^{+/-}$ *GCaMP6f*$^{+/-}$), mice homozygous for the Rosa-CAG-LSL-GCaMP6f::ΔNeo conditional allele (The Jackson Laboratory; B6;129S-*Gt(ROSA)26Sor*$^{tm95.1(CAG-GCaMP6f)Hze}$/J) were crossed with TRPM5-IRES-Cre mice (Kusumakshi et al., 2015). As control mice heterozygous or homozygous wildtype littermates were used, except for *Trpm5*$^{-/-}$ mice which were used for PTS measurements. In this case, C57BL/6J mice served as controls. Animals were anesthetized by isoflurane (5%) (Abbott) or carbon dioxide and killed by cervical dislocation or transecting the vena cava inferior.

Human samples

Patients with COPD (patient characteristics given in Figure S7A) were hospitalized because of exacerbation. Sampling of sputa was primarily undertaken for diagnostic purpose. Samples underwent routine bacterial screening; results are shown in Figure S7A. In addition, saliva and induced sputum (provoked by inhalation of 0.9%–10% saline for 15 min) were collected from 6 clinically inconspicuous volunteers. Two of them were positive for either *Haemophilus influenzae* or *Serratia marcescens* and, therefore, were excluded from further analysis. Characteristics of volunteers included in the study are given in Figure S7B. Aliquots of samples

were used for the purpose of this study upon receiving informed consent, as approved by the responsible ethics committee (Referenzvotum European IPF Registry: 111/08 Ethikkommission JLU Giessen Ad 3).

METHOD DETAILS

Peptides

Peptides were custom made by United Peptide, United BioSystems, Innovagen, GenScript Corparation, VCPBIO and Synpeptide. Peptides were chemically synthesized and purified (> 95%), which was verified by mass spectroscopy (MALDI-TOF) by commercial suppliers. Sequence, source and purity of each used peptide are listed in Table S5. Lyophilized peptides were dissolved as 1 mM stock solutions in buffer (130 mM NaCl, 10 mM HEPES, 5 mM KCl, 2 mM $CaCl_2$, 5 mM glucose (C1 Buffer)) and kept in small aliquots at −20°C until use. The sequences of the fMet peptides were designed according to motifs present at the N-termini of > 18,000 specific bacterial proteins annotated in UniProt database.

Bioinformatics

To analyze the natural occurrence and abundance in microorganisms of fMet peptides used in this study, we employed the peptide search function of UniProt. Further analyses concerning sequence, taxa, and function of specific organism were performed.

Measurement of particle transport speed

A modified version of the method previously described by Klein et al. (2009) was used. Tracheas were explanted and transferred in a delta T-dish coated with a thin layer of Sylgard polymer (Dow Corning) and submerged with HEPES (pH 7.4). Temperature (31°C) was controlled during the experiments using a Bioptechs Delta T micro-environmental control system (Bioptechs). The trachealis muscle was cut and the trachea was fixed flat on the bottom of the dish with needles. Before measurements (videos taken), polysterene dynabeads (Invitrogen) were added on the tracheal surface. The first measurement was done after 30 min of equilibration time, followed by measurements every 5 min until 55 min after start, then every 2 min. Stimulation (formylated peptides, LED) started after 59 min. LED stimulation was done for 2 min at 456 nm, 8 Hz and 60 ms pulse duration, using a UHP-T-DI-LED source (prizmatix), TTL pulse train generator (S/N 7276, Prizmatix) and a LED controller UHPLCC-T (Prizmatix) controlled by Prizmatix pulser software. Before each measurement, buffer and dynabeads were well mixed by pipetting. ATP (100 μM) was added 10 min before the end of each experiment and served as a viability control. Videos consisting of 200 images (640 × 51 pixels; 12 bit; 1 image per 84 ms) were taken using a UMPLFL20xW/0.5 water immersion objective (Olympus) and a SMX-150M (EHD imaging GmbH) camera. Movement of dynabeads was tracked and visualized by using Image-Pro Plus (MediaCybernetics) software, and the average speed of all tracked particles over a 15 s time period was calculated.

Measurement of ciliary beat frequency

Preparation of tracheas was done as described for PTS measurements, except that images were taken at higher magnification using an Olympus UMPLFL40xW/0.8 water immersion objective. Videos consisting of 1000 images with a frame rate of 105 images per second were taken before adding the formylated peptide f-MKKFRW (after 59 min of equilibration time) and every 2 min for 10 min, finally ATP (100 μM) was added. Mean CBF was calculated as describe before (Perniss et al., 2018), shortly dominating beat frequency of each ciliated cell (30-45 cells per video) was analyzed by fast Fourier transformation using a graphical User Interface for MATLAB R2016b which was programmed by Mario Pieper and Peter König (University of Lübeck, Germany).

Tissue fixation and immunofluorescence

Tissues were dissected and fixed by immersion in Zamboni solution (2% paraformaldehyde/15% saturated picric acid in 0.1 M phosphate buffer, pH 7.4) for at least 12 h. Fixed organs were washed in 0.1 M phosphate buffer and further processed for paraffin embedding, cryosectioning or whole-mount immunostaining. To obtain cryosections, specimens were immersed overnight in 0.1 M phosphate buffer with 18% sucrose, embedded in Tissue-Tek® O.C.T. (Sakura), snap frozen in cooled isopentane, and sectioned at 10 μm on a Microm HM560 cryostat. Paraffin sections (8 μm) were cut using a Leica RM2255 microtome. For immunohistochemistry of paraffin sections, antigen retrieval was performed using microwave treatment (2x5 min) in citrate buffer (pH 6.0). Cryo- and paraffin sections were further processed by saturating unspecific protein binding sites for 1 h in 0.005 M phosphate buffer containing 10% horse serum, 0.5% Tween 20, 0.1% bovine serum albumin (BSA). Primary antibodies directed against ChAT (RRID:AB_2079751, diluted 1:250), DCLK1 (RRID:AB_873537, 1:2,000), GFP (RRID:AB_10001164, 1:4,000), α-gustducin (RRID:AB_673678 from rabbit, 1:6,000; Covalab Cat#pab73402 from goat, 1:800), PLCβ2 (RRID:AB_632197, 1:800), Pou2f3 (RRID:AB_1855585, 1:400), TRPM5 (Kaske et al., 2007; 1:4,000), and villin (RRID:AB_2215974, 1:25), were diluted in 0.005 M phosphate buffer and applied overnight at 4°C. Then, sections were rinsed repeatedly, covered with fluorophore-conjugated secondary antibodies for one h at room temperature, rinsed, post-fixed with phosphate-buffered 4% paraformaldehyde and mounted in carbonate-buffered glycerol (pH 8.6) containing 1 μg/mL 4',5-diamidino-2-phenylindole (DAPI; Sigma Aldrich). For whole-mount immunostainings of tracheas, the trachealis muscle was cut longitudinally and opened tracheas were fixed flat with insect needles on a silicon elastomer. Specimens were permeabilized with 0.3% Triton X for 2 h, unspecific protein binding sites were saturated by incubation with 4% horse serum and 1% BSA in 0.005 M phosphate buffer for 2 h. Whole-mounts were incubated in primary and secondary antibodies overnight each at same concentrations as described above, except for anti-TRPM5 (1:8,000) and anti-CGRP (RRID: AB_2243858, used only at

whole-mounts; 1:3,000), rinsed, post-fixed for 10 min in phosphate-buffered 4% paraformaldehyde, and mounted in Mowiol (Sigma Aldrich) containing DAPI (1 μg/mL). Sections and whole mounts were evaluated by epifluorescence microcopy (Axioplan 2, Zeiss) or with a confocal laser scanning microscope (LSM 710, Zeiss). To quantify cholinergic chemosensory cells in the trachea, at least 6 tracheal cross-sections of each animal were evaluated and the number of positive cells per 2 mm basal lamina was calculated (Figure S1C-F). To quantify chemosensory cells in whole-mount preparations, at least 120 chemosensory cells per animal were analyzed (Figures S5F and S5H).

X-gal staining

ΔFpr3-lacZ mice carry a lacZ-tagged *Frp3* deletion allele (Bufe et al., 2019). Tracheal whole-mounts were prepared as described above. To stain the VNO, animals were killed by CO_2 inhalation followed by decapitation. The skin was removed from the skull, the mandible was removed and the cranium was opened by a sagittal cut, 1-2 mm lateral in parallel to the midline of the skull. Finally, the lateral aspect of the bony capsule of the VNO was opened with fine forceps. Afterward, tissues were fixed by immersion in 2% paraformaldehyde prepared in PBS, pH 6.9, overnight. Samples were equilibrated for 15 min each in PBS containing 2 mM $MgCl_2$ and 5 mM EGTA (buffer 1) and in PBS containing 2 mM $MgCl_2$, 0.01% sodium deoxycholate and 0.02% NP-40 (buffer 2). X-gal staining was performed overnight in the dark at 20°C by incubation in buffer 2 supplemented with 5 mM $K_3Fe(CN)_6$, 5 mM $K_4Fe(CN)_6$ and 1 mg/mL 5-bromo-4-chloro-3-indolyl-β-D-galactopyranoside (X-gal, stock solution 40 mg/mL in dimethylformamide). Bright-field images of X-gal stained whole-mount tissues were acquired on a SZX16 stereo microscope (Olympus) connected to a DP72 camera (Olympus) using "cellSens Dimension" software (Olympus). Images were assembled and adjusted in contrast and brightness using Photoshop Elements 10 (Adobe Photoshop).

Cell sorting and RT-PCR

Tracheas of three TRPM5-GFP mice were dissected, pooled, cut into small pieces and dissociated by incubation with papain (40 U/mL, Sigma Aldrich) and L-cysteine (25 mM, Sigma Aldrich) in tyrode 1 buffer without calcium chloride (140 mM NaCl, 5 mM KCl, 1 mM $MgCl_2$, 10 mM HEPES, 10 mM glucose and 1 mM sodium pyruvate) for 30 min at 37°C, as described previously (Krasteva et al., 2011). Tracheas were further dissociated by mechanically pipetting and digestion was stopped by addition of tyrode 2 buffer (1 mM $CaCl_2$, 140 mM NaCl, 5 mM KCl, 1 mM $MgCl_2$, 10 mM HEPES, 10 mM glucose and 1 mM sodium pyruvate) with leupeptin (5 mg/mL, Sigma Aldrich). The supernatant was removed und further dissociated by using a Cell Strainer (70 μm pore size, Sigma Aldrich). After centrifugation, the pellet was resuspended in MACSQuant Running Buffer (Miltenyi Biotec) containing 0.5% BSA. Cells were stained for 10 min at 4°C with fluorophore-conjugated primary antibodies against CD45 (Miltenyi Biotec, APC-Vio770 conjugate 130-1118-687) and CD326-EPCAM (Miltenyi Biotec, VioBlue-conjugate 130-102-421). Samples were FSC-A/SSC-A gated to exclude debris andFSC-H/FSC-A gated to select single cells. Dead cells were excluded by staining with propidium iodide. Cholinergic chemosensory cells were obtained by gating for $CD45^{low}$, $EPCAM^{high}$ and GFP^{pos}, epithelial cells were obtained by gating for $CD45^{low}$, $EPCAM^{high}$ and GFP^{neg} using a FACSAria III (BD Biosciences) and FACSDiva Software (BD Biosciences). After cell sorting, cells were centrifuged and mRNA was immediately isolated and cDNA synthesized using SuperScript III CellsDirect cDNA Synthesis System (Invitrogen) according to the manufacturer's protocol. Extracted RNA from tongue and VNO from ChAT-eGFP reporter mice using RNeasy Mini Kit (QIAGEN) served as positive control, samples without reverse transcriptase and PCR mix without cDNA served as negative control. PCR was performed by adding 1 μL of cDNA, 0.6 μL of each primer pair (10 pM, MWG, Biotech, primers provided in Table S6), 2.5 μL of 10x PCR buffer II (Thermo Fisher), 1.5 μL of $MgCl_2$ (Life Technologies), 0.5 μL dNTP (QIAGEN), 0.5 μL AmpliTaqGold polymerase (5 U/μL, Applied Biosystems) and 18.5 μL of H_2O. Cycling conditions were 5 min at 95°C, followed by 40 cycles of 45 s at 95°C, 30 s at 60°C, 45 s at 72°C, and a final extension at 72°C for 10 min. The PCR products were separated by electrophoresis on a 2% Tris-acetate-EDTA agarose gel.

Transfection and calcium imaging in HEK Cells

Functional analysis of Tas2r and Fprs was essentially done as described in Bufe et al. (2002, 2015). HEK293T (DSMZ # ACC-635) cells were seeded with 20%–30% confluence on poly-D-lysine-coated (10 μg/mL in PBS) black 96-well μCLEAR-plates (Greiner Bio-One). Twenty-four h later, cells were transfected using jetPEI (Polyplus-transfection SA) according to the manufacturer's protocol for 96-well transfections. For Ca^{2+} imaging experiments, cells were cotransfected with equal amounts of plasmids encoding a chemoreceptor and a promiscuous G_q-type G-protein α-subunit. G16-Gust44 was used for Tas2rs, and G16 for Fprs. Ca^{2+} signals to agonist stimulation were recorded 24 h post-transfection for Tas2rs and 48 h post-transfection for Fprs using the Ca^{2+} indicator dye Fluo-4/AM (Molecular Probes) and a fluorescence imaging plate reader (FLIPR) system (Molecular Devices). Mock controls were transfected with an empty pCDNA5 vector instead of the chemoreceptor and the appropriate G-protein α-subunit. Lyophilised peptides were routinely dissolved in the Ca^{2+} imaging assay buffer C1 (130 mM NaCl, 10 mM HEPES, 5 mM KCl, 2 mM $CaCl_2$, 5 mM glucose, pH 7.2) as 0.2–1 mM stock solutions and kept in small aliquots at −20°C until use.

Stimulation of tracheal acetylcholine release

Tracheas of C57BL/6J mice were dissected, placed in a glass dish covered with Sylgard polymer and fixed on silicon elastomer with needles. Surrounding tissue including nerves and fat was removed using a binocular. The trachealis muscle was cut longitudinally as described previously. The trachea was transferred to a 1.5 mL Eppendorf tube with 500 μL of HEPES buffer and incubated for 15 min at 37°C. Then, supernatant was collected to serve as control supernatant taken before stimulation. Next, 500 μL of HEPES buffer with

10 μM f-MKKFRW was added, incubated for 15 min and supernatant was removed. Supernatants were snap frozen in liquid nitrogen and stored at −80°C until further used for acetylcholine measurement by HPLC or Ca^{2+}-recording from reporter cells. Eserine (10 μM) was added throughout to all buffers to prevent breakdown of acetylcholine by endogenous cholinesterases.

For optogenetic stimulation, tracheas from ChAT-ChR2-YFP mice were dissected as described above, but then fixed on silicon elastomers. HEPES buffer containing eserine was directly added on top of the epithelium and incubated for 7 min at 37°C. Then, supernatant was removed and, again, HEPES buffer added. LED stimulation was done for 2 min with 456 nm, 8 Hz and 60 ms pulse duration, followed by 5 min additional incubation time. In experiments in which the epithelium was abraded, the trachea was prepared as described above. The epithelium was then removed before the LED stimulation by using a cotton swab, which was gently wiped over the tracheal surface. Supernatants were snap frozen and stored at −80°C until further processing.

Acetylcholine measurement by HPLC

Acetylcholine content in supernatants was analyzed as previously described (Lietsche et al., 2016) by microbore HPLC-ECD (high performance liquid chromatography-electrochemical detection) using the Eicom HTEC-500 system (Kyoto, Japan) that included degasser, low-speed pump, pre- and separation column, enzyme reactor carrying immobilised acetylcholine esterase and choline oxidase, and electrochemical detector with a platinum electrode operating at 500 mV relative to the Ag/AgCl reference electrode. The system was contained in a temperature controlled cabinet. Acetylcholine was retained on the separation column and cleaved to choline and acetate by acetylcholinesterase; choline was then oxidised to hydrogen peroxide by choline oxidase. Hydrogen peroxide was detected electrochemically. The mobile phase consisted of $KHCO_3$ 50 mM (Merck, Darmstadt, Germany), EDTA-2Na 134.3 μM (BDH, Poole, UK) and sodium decane-1-sulfonate 1.64 mM (Alfa Aesar, Karlsruhe, Germany) in RotisolV HPLC gradient grade water (Sigma-Aldrich, Munich, Germany), brought to pH 8.4. The flow rate was 150 μL/min. At an injection volume of 5 μL, the detection limit of this system was 1 fmol/injection. The intra-assay coefficient of variability ranged from 11 to 0.9% for injections of 1 to 700 fmol, whereas the inter-assay coefficient of variability amounted to 8%. Data acquisition was performed using EPC-500 PowerChrom software.

Acetylcholine measurement with reporter cells

M3WT4 cells (CHO-K1 cells expressing rat M3 muscarinic acetylcholine receptor) were freshly thawed for each experiment and seeded directly in Ham's F-12K (Kaighn's) medium (Thermo Fisher) supplemented with 10% FBS (Thermo Fisher), 1% Pen/Strep (Sigma Aldrich) on laminin (Invitrogen) and poly-L-lysine (Sigma Aldrich) coated glass coverslips (~20,000 cells per coverslip). Attachment of cells was achieved by incubating for 30-90 min. Cells were then loaded for 60-90 min with Fura 2-AM (8 μM, Thermo Fisher) in Ham's F-12K (Kaighn's) medium. Changes in intracellular calcium concentration $[Ca^{2+}]_i$ were recorded by digital microscopy with a Leica DM5000B equipped with an X-Cite 200DC illumination system (Waltham) for ratiometric recording of single cells. Coverslips were transferred into a Bioptechs Delta T dish and temperature (37°C) was controlled during the experiment. Cells were constantly perfused with Locke's solution (in mM: 136 NaCl, 5.6 KCl, 1.2 $MgCl_2$, 2.2 $CaCl_2$, 1.2 NaH_2PO_4, 14.3 $NaHCO_3$ and 10 mM dextrose, 37°C, pH 7.4). A field of cells was monitored by sequential dual excitation, 360 and 380 nm, the analysis of the image ratios was previously described (Božičević et al., 2017). Ratio images were acquired every second. Acetylcholine evoked a concentration-dependent increase in $[Ca^{2+}]_i$ (Figure S5A), which was fully inhibited by the muscarinic receptor antagonist, atropine (Figure S5B). In contrast, f-MKKFRW (10 and 100 μM) had no effect on $[Ca^{2+}]_i$ in isolated reporter cells (Figure S5C).

Supernatants of tracheas (100 μL) were added after 1 min of recording baseline $[Ca^{2+}]_i$, total volume in the dish was 1.5 mL. After application of supernatants, coverslips were washed for 3 min with Lockes's solution and acetylcholine (10^{-6} M) was added as a positive control. Changes in $[Ca^{2+}]_i$ were calculated in respect to average baseline level within 15 s prior application of supernatants and only cells which react upon stimulation by either supernatant or acetylcholine were evaluated. Each supernatant was tested twice in independent experiments.

Ca^{2+}-Recording in sensory neurons

To obtain isolated sensory neurons from the jugular-nodose complex, the skull of *Chrna3*-eGFP mice was opened and the brain and the inner ears were removed. Then, the roots of the vagal nerve were identified and traced to the jugular-nodose ganglion complex. This was dissected and transferred into HBSS (Thermo Fisher) supplemented with 2 mg/mL of each dispase (Sigma Aldrich) and collagenase A (Sigma Aldrich). The tissue was dissociated with glass pipettes and incubated for 60 min at 37°C. Subsequently, cells were washed with L-15 medium supplemented with 10% FBS (Thermo Fisher) and 1% Pen/Strep (Sigma Aldrich). Cells were seeded on laminin (Invitrogen) and poly-L-lysine (Sigma Aldrich) coated glass coverslips and incubated overnight in L-15 medium. The coverslips were washed and loaded with Fura-2 AM (8 μM) for 30-90 min. For measurements of changes in intracellular Ca^{2+}, the same hardware setup was used as described above. Two independent experiments with 3 animals each were conducted. From each of these animals, neurons were seeded on 3-4 coverslips. Shown data display pooled results from all animals and both experiments. Only cells which were GFP positive and reacted to either nicotine or capsaicin were evaluated. During the experiment, cells were continuously perfused with Lockes's solution and washed for 2 min between application of stimuli.

Ca^{2+} Imaging of $TRPM5^+$ cells in whole-mounts

Mice (5-14 weeks old, either sex) were anesthetized by i.p. injection with 165 mg/kg body weight ketamine (Pharmacia GmbH, Berlin, Germany) and 11 mg/kg body weight xylazine (Bayer Health Care, Leverkusen, Germany) according to institutional guidelines.

Tracheas were dissected and transferred to a solution containing 140 mM NaCl, 5 mM KCl, 1 mM $MgCl_2$, 2 mM $CaCl_2$, 10 mM HEPES, adjusted to pH 7.4. The respiratory epithelium was exposed by cutting the trachea along the tracheal muscle. During Ca^{2+} imaging, the preparation was kept in the same bath solution as in the PTS experiments containing 136.4 mM NaCl, 5.6 mM KCl, 1 mM $MgCl_2$, 2.2 mM $CaCl_2$, 10 mM HEPES, adjusted to pH 7.4, and 10 mM glucose (300 mOsm). Chemostimuli were freshly prepared each day and diluted in bath solution to give the following final concentrations: f-MKKFR (50 μM), f-MKKFRW (50 μM), cycloheximide (100 μM, and 10 mM), denatonium benzoate (100 μM and 10 mM). Stimuli were applied successively through the bath. A Ca^{2+} response was defined as a stimulus-evoked deviation of GCaMP6f fluorescence that exceeded twice the SD of the mean of the baseline fluorescence noise, with a minimal duration of 10 s or containing at least 3 Ca^{2+} spikes at a frequency of 0.1 Hz. In time series experiments, ligand application was repeated to confirm repeatability of a given response. GCaMP6f Ca^{2+} imaging methodology was adapted (Trouillet et al., 2019) but using a Leica TCS SP5 confocal microscope with a 20x 1.0 water-immersion objective (HCS APO L) (Pyrski et al., 2017; Bufe et al., 2019). Excitation wavelength was 488 nm and emitted fluorescence was collected between 500 and 550 nm. All scanning head settings were kept constant during each experiment. Optical sections were approximately 9 μm thick. Fluorescence changes are expressed as relative fluorescence changes, i.e., F/F_0 (with F_0 as the average of the fluorescence values during control stimulation with extracellular bath solution). Images were acquired every 1.29 s and analyzed using Fiji (NIH), Igor (Wavemetrics) and Originlab (Origin) software.

Force recordings in organ bath

Tracheas from ChAT-ChR2-YFP and *Avil^{cre}:Chat$^{fl/fl}$* mice were explanted and a segment consisting of 3-4 cartilage rings was taken from the mid-region. Urinary bladders from ChAT-ChR2-YFP mice were explanted and longitudinally divided into two pieces. Isometric contraction was measured by mounting the specimens in vertical 15 mL glass chambers of a computerized isolated organ bath system (ADIinstruments). The chambers were perfused with MEM-Medium (37°C, pH 7.4) (Thermo Fisher) supplemented with 1% penicillin/streptomycin (PAA) and constantly aerated with 95% O_2/5% Co_2 gas mixture. Two stainless steel hooks were inserted into tracheal rings to record radial tension, and bladder strips were by mounted between to stainless steel clips. The proximal stainless clip was connected to an isometric transducer (Power Lab 8.30, ADInstruments). Tissues were placed between paddles for EFS and equilibrated against a passive load of 0.5 g tension. Changes in the isometric contraction were converted by the transducer into an amplified DC output voltage and assigned to the software LabChart 6 (ADInstruments GmbH, Heidelberg, Germany). All samples were equilibrated for 30 min until they reached a stable baseline tension. After further 10 min, tissues from ChAT-ChR2-YFP were stimulated with LED for 2 min (456 nm, 8 Hz and 60 ms pulse duration). At the end of each experiment, EFS (150 mA, 10 V, 30 s pulse trains at 1, 8 and 16 Hz, respectively, with 2 min interval between stimulation trains) was applied by an Multiplex PulseBooster (Ugo Basile) and served as reference and viability control. Tracheas of *Avil^{cre}:Chat$^{fl/fl}$* were stimulated with EFS (150 mA, 10 V, 1 min pulse trains at 10 Hz) for 1 min and again after 5 min (EFS 1). After 5 min, vehicle control (DMSO) was added and a second train of EFS applied (EFS 2). Then, atropine (1 μM) was added, and a third EFS followed after 5 min (EFS 3). KCl (50 mM) was administered at the end of each experiment and served as viability control. Changes in tension were recorded as force, measured in grams.

Bacterial supernatants

Supernatants from MgrB overexpressing bacteria were essentially obtained as described in (Bufe et al., 2019). The plasmid pmgrB-H6 containing the entire coding region of *E. coli mgrB* (GenBank Z2872) fused to a C-terminal His-6 tag was transformed into *E. coli* BL21 (DE3) pLysS (NEB) and plated on ampicillin (100 μg/mL) containing LB agar plates. After 16–24 h incubation at 37°C, freshly grown colonies were transferred to 30 mL 1x M9 Salt Solution (Sigma-Aldrich) supplemented with 1x MEM Amino Acid Solution (Sigma-Aldrich). After 24–48 h growth at 37°C, this bacterial culture was harvested by centrifugation and resuspended in fresh M9 medium supplemented with 1x MEM Amino Acid Solution and 0.1 mM isopropyl β-D-1-thiogalactopyranoside (Sigma-Aldrich). After 24 h growth at 37°C, 10 mL samples were collected. Bacteria were harvested by centrifugation. The remaining supernatant was collected, heat-inactivated for 10 min at 80°C, immediately frozen and stored at −20°C until use.

MALDI-TOF mass spectrometry of human samples

Samples were treated with Sputasol® according to the manufacturer's protocol. Then, 1 mL of each sample was acidified with trichloroacetic acid to a final concentration of 12% (w/v) (Merck, Darmstadt, Germany), incubated on ice for 15 min and clarified by centrifugation for 15 min at 15,000 rpm and 4°C. As positive controls, pure peptides dissolved in C1 buffer were used and handled identical to human samples except Sputasol® treatment. The samples were loaded onto an activated C18-SPE cartridge (100 mg; Macherey-Nagel, Düren, Germany). The retained peptides were washed with 0.1% TFA, eluted with 80% acetonitrile (Roth GmbH, Karlsruhe, Germany) in 0.1% TFA and lyophilised overnight. Afterward, samples were redissolved in 20 μL 0.1% TFA, and 1 μL of this sample was mixed with 1 μL matrix solution (2,5-dihydroxybenzoic acid, DHB; 5 mg/mL; Sigma, Darmstadt, Germany), and methylendiphosphonic acid (MDPA; 5 mg/mL; Fluka, Steinheim, Germany) in 0.1% TFA) for MS analysis. MALDI-TOF-MS was performed on an Ultraflex I TOF/TOF mass spectrometer (Bruker Daltonics, Bremen, Germany) equipped with a nitrogen laser and a LIFT-MS/MS facility. The instrument was running in the positive-ion reflectron mode, acquiring 200–400 single spectra per sample for sum spectra. For data processing and instrument control, the Compass 1.3 software package consisting of FlexControl 2.4, FlexAnalysis 3.0, BioTools 3.0 was used.

Bacteriological investigation of mouse colony

To investigate the colonization of *Trpm5*$^{-/-}$, *Trpm5*$^{+/-}$ and *Trpm5*$^{+/+}$ mice with *B. pseudohinzii,* samples were taken under aseptically conditions from mice of both sexes and processed as described in Perniss et al. (2018). The proximal part of the trachea (2-3 rings) and the right caudal lung lobe, each sample weighing around 20-40 mg, were dissected. The pharynx sample was taken by wiping with a cotton swab (Nerbe plus, Winsen, Germany). Each sample was examined by streaking onto blood agar plate (Oxoid GmbH, Wesel, Germany), on brain heart infusion (BHI) agar (Oxoid GmbH, Wesel, Germany) and selective agar plates (blood agar containing cephalexin hydrate (20 mg/mL; Sigma Aldrich); nutrient broth no. 2 and agarose containing neomycin trisulfate salt hydrate (2 mg/mL; Sigma Aldrich) and bacitracin (3 mg/mL; Carl Roth, Karlsruhe, Germany); water-blue metachrome-yellow lactose agar (acc. to Gassner, E. Merck). For enrichment purposes, each sample was inoculated to nutrient broth no. 2 containing 10% bovine serum, and after 24 h of incubation at 37°C this broth was streaked onto blood and Gassner agar plates. Plates were examined after 24 h and 48 h, as well as for BHI agar after 72 h of incubation at 37°C. Semiquantitative analysis of bacterial growth of *B. pseudohinzii* was evaluated blinded with no knowledge of the genotype, using a scoring system. Score 0: No *B. pseudohinzii* colonies could be observed in the directly plated tissue homogenate or in the overnight culture. Score 1: Overnight culture was positive and/or 5-50 colonies were observed after direct plating. Score 2: Overnight culture was positive and 50-200 colonies were observed after direct plating. Score 3: more than 200 colonies. The colonies were counted either on the blood agar plates or selective agar plates. If the cultures were grown on blood agar plates, they were subsequently cultured on selective agar plates to ensure identification as *B. pseudohinzii*, and pure cultures were identified using MALDI-TOF MS (Biotyper Version V3.3.1.0, Bruker Daltonics, Bremen, Germany) and the DB 5989 database.

QUANTIFICATION AND STATISTICAL ANALYSIS

All experiments were performed using randomly assigned mice with partial investigator blinding. Statistical details of experiments are specified in the figure legends. All data points and "n" values reflect biological replicates (i.e., mice), except in Figures 5B and 5C, where one data point reflects the mean of two independent experiments. No data were excluded, except experimental samples did not respond to the positive and viability controls at the end of the experiment (i.e., positive response to ATP for PTS, stimulatory effect of EFS in organ bath recordings, and positive response to acetylcholine and capsaicin for $[Ca^{2+}]_i$ recording in M3WT4 cells and sensory neurons, respectively). Statistical analysis was performed as noted in figure legends using Prism 7 (GraphPad) software. Datasets for acetylcholine release followed normality of distribution and, therefore, were analyzed by parametric tests, whereas distribution of PTS data significantly deviated from normal distribution and were analyzed by non-parametric tests.

DATA AND CODE AVAILABILITY

This study did not generate any unique datasets or code.